Polarization effects in the ionization cross section of Ar, Kr, and Xe by laser-excited Ne**[(2p)5(3p);J = 3, M] atoms

Polarization effects in the ionization cross section of Ar, Kr, and Xe by laser-excited Ne**[$(2p)^5(3p);J=3,M$] atoms

J. P. J. Driessen,* F. J. M. van de Weijer, M. J. Zonneveld, L. M. T. Somers, M. F. M. Janssens, H. C. W. Beijerinck, and B. J. Verhaar

Physics Department, Eindhoven University of Technology, P.O. Box 513, 5600 MB Eindhoven, The Netherlands

(Received 20 July 1989)

In a crossed-beam experiment the total ionization cross section for the title systems has been investigated in the range $0.1 \leq E$ (eV) ≤ 4 of collision energies. The population of the short-lived Ne**[$(3p);J=3$] state is produced by saturated optical pumping of the Ne*[$(3s);J=2$]$\leftrightarrow$Ne**[$(3p);J=3$] two-level system with a polarized laser beam, resulting in a well-determined distribution of the magnetic substates $|J,M\rangle$ with respect to the relative velocity **g**. By measuring the ion yield in the scattering center at five different orientations of the laser polarization (linear and circular) with respect to **g**, the data can be analyzed in terms of pure-state total ionization cross sections ${}^3Q^{|M|}$ corresponding to a single asymptotic state $|J,M\rangle$. The observed polarization effect at $E=0.1$ eV is ${}^3Q^{|M|=0,1}/{}^3Q^{|M|=3}=2.5$, which is in good agreement with the data of Bussert, T. Bregel, R. J. Allan, M. W. Ruf, and H. Hotop [Z. Phys. A **320**, 105 (1985)] in the thermal energy range as obtained by analyzing the Penning electrons. This polarization effect decreases to a value of 1.4 for $E>2$ eV. The results are discussed in terms of semiclassical scattering calculations with an optical potential as input, using a model-potential approach for calculating both the real and the imaginary parts. For the autoionization width this results in a two-state $\Gamma_{\sigma'}$ and $\Gamma_{\pi'}$ basis for the σ' and π' orientations of the $(2p)^{-1}$ hole, calculated in a one-electron orbital overlap approximation. The preference for the $\Omega=0,1$ states at $E=0.1$ eV indicates the correct relative scaling of these two ionization widths, leading to $\Gamma_{\sigma'}=79\Gamma_{\pi'}$ at $R=4.5a_0$. The observed energy dependence is due to the decrease of "locking" of the total angular momentum **J** to the internuclear axis **R** with increasing angular velocity $\dot{\phi}$, leading to the dynamical criterion $\omega_{\text{prec}}=4\dot{\phi}$ for the transition of a space-fixed to a body-fixed description of **J**. The semiclassical precession frequency ω_{prec} of **J** around **R** is related to the average Ω splitting of the real part of the optical potential by $\omega_{\text{prec}}=\langle \Delta V_{\Omega,\Omega\pm1}\rangle/\hbar$. With these assumptions we observe a good agreement between the experimental results and the semiclassical calculations. Finally, we discuss the validity of a semiclassical locking picture, with emphasis on the difference between locking of the angular momentum versus locking of the electron orbitals involved.

I. INTRODUCTION

Scattering experiments with polarized atoms have become possible with the availability of stabilized cw single-mode dye lasers. The alignment of the excited atom with respect to the initial relative velocity **g** is determined by the laser polarization. Polarization effects as a function of the angle between laser polarization and relative velocity have been observed in (Ca,Sr)–rare-gas spin-changing collisions [$I_{\max}/I_{\min}=Q_{\max}/Q_{\min}=1.2$ to 2.5 (Refs. 1–4)] and in ionizing collisions of excited Ne states with Ar [$I_{\max}/I_{\min}=1.33$; $Q_{\max}/Q_{\min}=1.8$ (Refs. 5 and 6)]. The interpretation of the observed polarization effect [$I_{\max}/I_{\min}$] in terms of cross sections for the different magnetic substates [$Q_{\max}/Q_{\min}$] is not always straightforward, as can be seen in the case of associative ionization of two Na($3p$) atoms [$I_{\max}/I_{\min}=2$; negative Q values (Ref. 7)]. Very large polarization effects ($I_{\max}/I_{\min}=Q_{\max}/Q_{\min}=5$ to 10) occur in the case of intramultiplet mixing of short-lived Ne**[$(2p)^5(3p)$] atoms colliding with He.[8–10]

Many interesting features of the potential surfaces and collision dynamics can be obtained from these polarization effects. A full quantum-mechanical analysis is the proper way and has been successfully applied in one case.[8] It is a rather elaborate calculation with little gain in insight in the collision dynamics. Semiclassical models, although not fully correct, have proven so far to give more insight into the ongoing collision dynamics.[10] A very interesting feature in a semiclassical analysis is the concept of "locking".[10–17] During a collision the two atoms pass through regions where different coupling schemes apply.[18,19] The interpretation of this phenomenon in terms of "orbital locking" is a hot topic in the recent literature. There are both arguments for[10–15] as well as against[16,17] this "locking" picture, with an angular momentum (**J**, **L**, or **S**) going from a space-fixed situation to a body-fixed situation.

The interpretation of the observed polarization effects in the underlying inelastic processes is very sensitive to this locking picture.[6] Therefore a clear picture of the applied locking interpretation must be given when analyzing polarization effects.

Our primary aim is to study the polarization effects in

the ionization cross section of the Ne**[(3p);J=3]-(Ar,Kr,Xe) systems in the energy range $0.05 < E$ (eV) < 6. This wide energy range is essential because it allows us to separate the influence of locking from the actual energy dependence of the process of ionization. The choice of the Ne**[(3p);J=3] short-lived state is determined by the requirements of sufficient ion intensities. Although the state is short lived ($\tau \approx 20$ ns), this state is the upper level of the Ne*[(3s);J=2]↔Ne**[(3p);J=3] two-level system, with a metastable lower level. By saturated laser excitation both states become nearly equally populated. This also results in an additional problem in analyzing the data. Due to the repeated excitation, both the upper *and* the lower level become polarized. For a correct analysis of the upper-state polarization effect, it is thus essential to perform a separate measurement of the polarization effect in the ionization cross section of the metastable lower state. The only data available for this polarization effect are of Bregel *et al.*[20] for the energy range $30 < E$ (meV) < 150 and of Driessen *et al.*[21] in the energy range $50 < E$ (meV) < 5000.

The process of Penning ionization is usually described in terms of an optical potential, which consists of a real part $V(R)$ determining the classical trajectory, and an imaginary part, the so-called autoionization width $\Gamma(R)$. In Sec. II we discuss the model-potential method for calculating $V(R)$ and extend this approach to the imaginary part $\Gamma(R)$. In this way a rather simple expression for $\Gamma(R)$ is obtained, which can be applied to both the metastable and the short-lived states with the advantage of a rather limited number of free parameters.

The experiments have been performed in a crossed-beam machine (Sec. III), with a well-defined relative velocity vector **g**. The process of optical pumping produces a distribution of magnetic substates with respect to the laser quantization axis (electric field **E** or wave vector **k**), which has to be transformed to the quantization axis **g** which is relevant for the collision process. Both the process of optical pumping and this transformation are discussed in Sec. IV.

In Sec. V we discuss the experimental signals that we obtain in our measurements of the polarization effect in the ionization cross section. In Sec. VI we present measurements of the polarization effect in the ionization cross section of the short-lived upper level. To obtain a high accuracy we have first sacrificed the energy resolution, presenting data at the average energies of the two beam sources used being $E = 130 \pm 50$ meV and $E = 2500 \pm 1500$ meV. This allows a detailed and direct comparison with the Penning ionization electron spectroscopy data of Bussert at thermal energies.[5] The polarization effects have also been studied including energy resolution (Sec. VII). In this case we analyze the influence of the polarization effect of the Ne*[(3s)] lower level on the polarization effect of the Ne**[(3p)] upper level.

In Sec. VIII we discuss the observed differences for the Ne*[(3s)] and Ne**[(3p)] states in terms of a semiclassical locking model for the rotational coupling of the total electronic angular momentum **J** and the dynamics of the ionization process in terms of our model-potential approach for the autoionization width $\Gamma(R)$. The competing process of intramultiplet mixing has also been included in these semiclassical model calculations, using an approach similar to that of Manders *et al.*[10] for the Ne**-He system.

II. DYNAMICS OF PENNING IONIZATION

A. Model potentials

The process of Penning ionization is usually described by an optical potential $V_{\text{opt}}(R)$ given by

$$V_{\text{opt}}(R) = V(R) - \tfrac{1}{2} i \Gamma(R) . \tag{1}$$

The real part $V(R)$ determines the classical trajectories and the autoionization width $\Gamma(R)$ takes into account the loss of flux due to ionization. In a classical interpretation the ionization rate at an internuclear distance R is equal to $\Gamma(R)/\hbar$.

Ab initio calculations of the potential curves involve all electrons, e.g., for the Ne**-Ar system a total of 28 electrons.[22,23] The model-potential method, which only considers the motion of the valence electron in the effective potential of the two cores, is much less laborious.[24,25] It has been successfully applied to generate adiabatic potential curves for the Na-Ne system[24] and the Ne**-He system.[8,25] In the latter case the nonisotropic interaction with the $(2p)^{-1}$ core of neon has to be taken into account as well. The same holds for the Ne**-Ar system.

Firstly, the one-electron Schrödinger equation is solved for the isotropic part of the interaction with the Ne^+ core without spin-orbit interaction, which results in a two-dimensional basis $V_\sigma(R)$ and $V_\pi(R)$ for the $|(3p);|m_\ell| = 0,1\rangle$ states of the valence electron. Because the actual atomic states $|LSJM_J\rangle$ are not pure σ or π states, the matrix elements of the one-electron interaction are linear combinations of $V_\sigma(R)$ and $V_\pi(R)$. The adiabatic potential curves of the molecular system are then obtained by diagonalization of the total Hamiltonian, including the spin-orbit coupling and the nonspherical part of the valence electron-core interaction of the neon atom.

To determine the basis potentials for the $(3s,3p)$ valence electron in the Ne**[$(2p)^5(3s,3p)$]-Ar molecular system, we use the potential moments calculated by Düren *et al.*[26] for the Na(*)[$(2p)^6(3s,3p)$]-Ar system. The electronic configuration of the Ne atom and the Na atom are identical, except for the $(2p)^{-1}$ core in the neon case. This results in an additional anisotropic interaction, which becomes noticeable only at short internuclear distances R. The Hartree-Fock wave functions for Ne and Na are almost identical,[27] therefore we use the Na(*)[$(2p)^6(3s,3p)$]-Ar potential curves $V_\sigma(R)$ and $V_\pi(R)$ for the Ne*(*)-Ar system. The extra potential splitting $V^{\text{core}}(R)$, due to the anisotropic core configuration, is based on the Ne^+-Ar system,[28] as given by

$$V^{\text{core}}(R) = 990 \text{ (eV)} \exp(-2.03 a_0^{-1} R) . \tag{2}$$

The potentials for the core interactions are now given by

$$V_{\sigma'}^{\text{core}}(R) = -\tfrac{2}{3}V^{\text{core}}(R)\ ,$$
$$V_{\pi'}^{\text{core}}(R) = \tfrac{1}{3}V^{\text{core}}(R)\ . \tag{3}$$

We have constructed the real potential curves using the recipe of the model-potential method of Hennecart and Masnou-Seeuws.[24,25] The contribution of the anisotropic Ne$(2p)^5$ core has been taken into account according to the extension of the model-potential method as described by Manders *et al.*[8] The input potential curves are $V_\sigma(R)$ and $V_\pi(R)$ for the Ne$(3p)$-Ar interaction and $V_{\sigma'}^{\text{core}}(R)$ and $V_{\pi'}^{\text{core}}(R)$ for the Ne$(2p)^5$-Ar core interaction. We thus obtain adiabatic potential curves for all Ne$^{**}[(2p)^5(3p);J\Omega]$-Ar states, with Ω the absolute value of the magnetic quantum number of the total angular momentum J with respect to the internuclear axis. The real potential curves we have thus constructed for the Ne$^{**}[(2p)^5(3p);J=3,\Omega]$-Ar system are depicted in Fig. 1. As already noted by Bussert *et al.*,[5,6] the repulsive barrier of Ne$^{**}[J=3,\Omega=0^-]$-Ar potential is the result of an avoided crossing with Ne$^{**}[\alpha_7,J=1,\Omega=0^-]$-Ar potential with α_k the $2p_k$ state in Paschen notation. In our semiclassical calculations (Sec. VIII), we have included Landau-Zener transitions between the neighboring states with $\Omega=0^-$: $\alpha_9(J=3)\leftrightarrow\alpha_7$. The intermediate maximum in the Ne$^{**}[J=3,\Omega=0^-]$-Ar potential curve has been confirmed in the Penning ionization electron spectroscopy (PIES) experiments of Bussert *et al.*[5] and Bregel *et al.*[20] The Ne**-Ar potentials are almost the same as the ones Bussert calculated,[5,6] only the repulsive wall of the potential lies at shorter internuclear distances in our case. This difference originates from the fact that Bussert takes into account the $(3s)$ contribution in the calculation, which we neglected. The repulsive branch of the potentials is not reliable, because it is very difficult to obtain a complete basis set *and* because the model-potential method loses its validity in this R range. For a comparison we have depicted the best available Ne$^*[(3s)]$-Ar potential of Gregor and Siska[29] as well. It has been shown that this potential gives a good description of elastic differential cross sections at thermal energies[29] and total scattering cross sections in a wide energy range.[30]

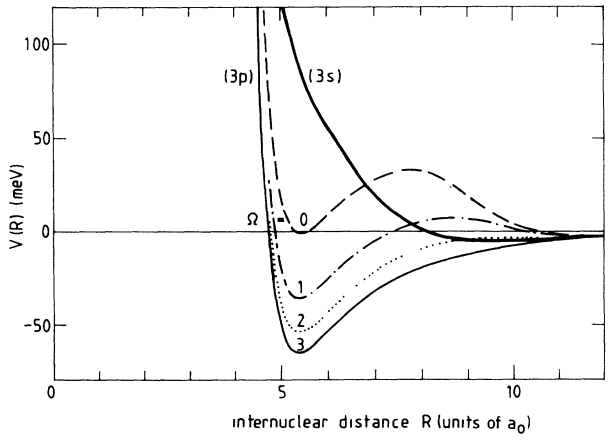

FIG. 1. The real potential curves $V_\Omega(R)$ for the Ne$^{**}[(2p)^5(3p);J=3]$-Ar system, calculated with the model-potential method of Hennecart and Masnou-Seeuws (Refs. 24 and 25) in combination with the $(3p)$ input potentials of Bussert *et al.* (Refs. 5 and 6), in comparison with the best available Ne$^*[(3s)]$-Ar potential of Gregor and Siska (Ref. 29).

B. Autoionization width

To determine the R dependence of the autoionization width $\Gamma(R)$ of the optical potential, we have to obtain insight in the mechanism of the process of ionization. Two mechanisms have been proposed:[29,31] a radiative mechanism and an exchange mechanism. In the radiative mechanism the excited Ne$^{*(*)}$ state decays to the ground state, accompanied by the promotion of an electron of the target atom to a free-electron state in the continuum. In the exchange mechanism an electron of the target atom is transferred to the $(2p)^{-1}$ hole of the neon atom, with a simultaneous transition of the excited valence electron to a free-electron state. The excited Ne$^{*(*)}$ states that we deal with are pure triplet states. Because of the optical selection rules, the radiative mechanism can be neglected and the exchange mechanism is expected to be dominant.[29]

A full calculation of the autoionization width requires the calculation of two-electron two-center integrals, which takes into account the two electrons involved in both the initial and final state.[32,33] This rigorous approach has been put into practice,[34,35] e.g., for the He*-(H,D) system. A commonly used approximation for the autoionization width $\Gamma(R)$ is the squared overlap integral of the two orbitals involved in the first step of the exchange mechanism, i.e., the transfer of a target electron to the $(2p)^{-1}$ hole of neon. For the Ne$^{*(*)}$-Ar system both orbitals are p orbitals and thus this overlap integral is orientation dependent. We can discern two orientations $|(2p)^{-1},|m_\ell|=0,1\rangle$ of the core, resulting in a two-state basis $\Gamma_{\sigma'}(R)$ and $\Gamma_{\pi'}(R)$. For the radial part of the atomic wave function we have used the wave function of Clementi[36] for Ar$(3p)$ and the wave function of Haberland[37] for Ne$(2p)$; for the angular part of the usual spherical harmonics have been used. With these oriented wave functions we have calculated the squared overlap integrals, denoted as $\Gamma_{\sigma'}$ and $\Gamma_{\pi'}$. These autoionization widths are depicted in Fig. 2, with the corresponding orientations of the orbitals involved given in the inserts. We observe that both autoionization widths can be described in good approximation by a single exponential function with a cutoff at small internuclear distances, in agreement with experimental evidence.[38–40] Of course, a sharp nonanalytical cutoff represents a nonphysical behavior. In general, the accuracy of experimental information is not sufficient to determine more detail such as a smooth transition to saturation. Only for a limited number of cases can this be done.[35] Secondly, we remark that $\Gamma_{\pi'}(R)$ falls off more rapidly, because both the radial and the angular dependence of the orbitals involved influence the R dependence. Because the electron that makes a transition to a free-electron state in the exchange mechanism has not been taken into account, the absolute value of both functions and their scaling relative to each other

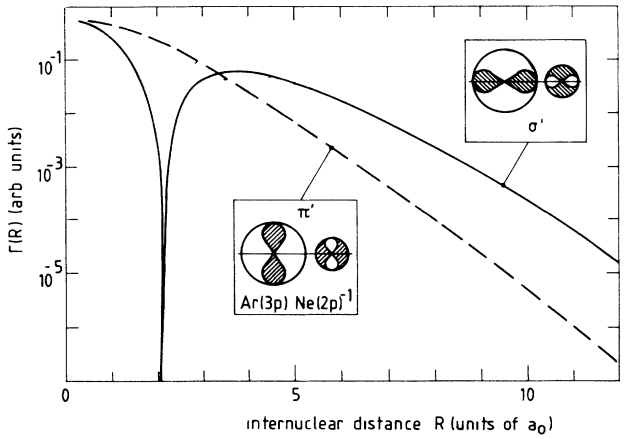

FIG. 2. The calculated two-state basis set $\Gamma_{\sigma'}(R)$ and $\Gamma_{\pi'}(R)$ for the autoionization width whose elements are proportional to the squared overlap $|\langle \mathrm{Ne}(2p)^{-1}, m_\ell | \mathrm{Ar}(3p), m_\ell \rangle|^2$ ($m_\ell = 0, \pm 1$). The inserts show the two configurations of projectile and target orbitals that contribute. The scaling of the two autoionization widths relative to each other is undetermined because the influence of the second electron on the matrix element has not been taken into account.

is still undetermined. This overlap calculation only gives information on the shape of the functions. The range of validity is estimated at $R > 5a_0$, which is based on the molecular wave-function calculations of Hennecart and Masnou-Seeuws.[24,25]

As discussed in the model-potential approach, the adiabatic atomic $|LSJM_J\rangle$ states and the adiabatic molecular $|J,\Omega\rangle$ states are thus linear combinations of both basis functions. Moreover, a detailed analysis of the autoionization width in terms of the Feshbach formalism shows that in the local approximation the autoionization width is diagonal in the quantum number Ω.[32,33] This results in

$$\Gamma_{J\Omega}(R) = c_{\sigma'}(R)\Gamma_{\sigma'}(R) + [1 - c_{\sigma'}(R)]\Gamma_{\pi'}(R) \ . \qquad (4)$$

The weight factor $c_{\sigma'}(R)$ is the squared amplitude of the σ' contribution to the wave function of the $|J,\Omega\rangle$ state, i.e., the relative population. For both excited states Ne*[(3s);$J=0,2$] and Ne**[(3p);$J=3$], the weight factors $c_{\sigma'}$ for pure atomic conditions are given in Table I. For the Ne*[(3s);$J=2$] and the Ne**[(3p);$J=3$] states the spin and orbital angular momentum of the core and the valence electron are all aligned, resulting in a gradual decrease of the σ' character of the Ne$^{*(*)}$ state with increasing Ω values. For the Ne*[(3s);$J=0$] state an isotropic mixture of σ' and π' character is observed.

This new approach to the autoionization width proves to be very valuable in explaining the ionization cross section for both metastable states and short-lived electronically excited states, as discussed in Secs. II C and VIII.

C. New light on metastable atom ionization cross sections

The two metastable states Ne*[(3s);$J=0,2$] both have a (3s) valence electron and an oriented $(2p)^{-1}$ core. In a collision experiment of unpolarized Ne*[(3s)] atoms both metastable states will have an randomly oriented $(2p)^{-1}$ core. This would result in the same cross sections ^0Q and ^2Q for both Ne*[(3s);$J=0,2$] states. State-selected experiments using a laser beam technique, however, show a 30% larger ionization cross section ^0Q for the Ne*[(3s);$J=0$] state in the thermal energy range increasing to 50% in the superthermal energy range.[38] Despite all experimental and theoretical effort in the past 15 years, this cross-section difference has remained as one of the unsolved basic problems.[41–43] The cross-section ratio $^0Q/^2Q$ can be explained by a difference in either the real part and/or the imaginary part of the optical potential. It is generally accepted that the difference in the real potential $V(R)$ for the two Ne*[(3s)] states is negligible.[42] A difference in the imaginary part $\Gamma(R)$ seems to be obvious. However, there is no mathematical evidence for a difference in the autoionization width as of yet. We will discuss the influence of the imaginary part in detail, using the model autoionization width of Eq. (4) as starting point.

TABLE I. The relative populations $c_{\sigma'}$ of the $(2p)^{-1}$ core for the atomic Ne$^{*(*)}[J,\Omega]$ states.

	$\Omega=0$	$\Omega=1$	$\Omega=2$	$\Omega=3$
Ne**[(3p);$J=3$]	$\frac{9}{15}$	$\frac{8}{15}$	$\frac{5}{15}$	0
Ne*[(3s);$J=2$]	$\frac{2}{3}$	$\frac{1}{2}$	0	
Ne*[(3s);$J=0$]	$\frac{1}{3}$			

An important observation is that the spherical average of the weight factors $c_{\sigma'}(\Omega)$ for the Ne*[(3s);$J=2$] state, given by $\langle c_{\sigma'} \rangle = \frac{1}{5}\{c_{\sigma'}(\Omega=0) + 2c_{\sigma'}(\Omega=1) + 2c_{\sigma'}(\Omega=2)\}$, is equal to the value of $c_{\sigma'}(\Omega=0)$ for the Ne*[(3s);$J=0$] state, as follows directly from the underlying vector algebra. This implies that, independent of the shape and magnitude of $\Gamma_{\sigma'}(R)$ and $\Gamma_{\pi'}(R)$, the spherical average of the $\Gamma_{J\Omega}(R)$ functions of the Ne*[(3s);$J=2$] state, given by $\Gamma_2(R) = \frac{1}{5}\{\Gamma_{20}(R) + 2\Gamma_{21}(R) + 2\Gamma_{22}(R)\}$, is also always equal to the autoionization width $\Gamma_0(R)$ of the Ne*[(3s);$J=0$] state. This does not imply, however, that the ionization cross section ^2Q for a nonpolarized beam of Ne*[(3s);$J=2$] atoms is equal to the cross section ^0Q for unpolarized Ne*[(3s);$J=0$] atoms. The full dynamics of the collision, which is essentially nonlinear in the autoionization widths $\Gamma_{J\Omega}$, enters this last step.

As already stated in Sec. II B, the relative scaling of the basis functions $\Gamma_{\sigma'}(R)$ and $\Gamma_{\pi'}(R)$ is still undetermined. A choice has to be made for this scaling factor, based on experimental evidence: the ratio $^0Q/^2Q$, the polarization effects $^2Q^{|M|}/^2Q$, or the fine-structure branching ratio of the Ar^+ final states. According to the analysis of Morgner,[42] the autoionization width is proportional to the squared matrix elements $|u_{m',m}|^2$, with the indices referring to the magnetic quantum numbers of the Ne$(2p)^{-1}$ hole and the Ar(3p) core electron. Based on the experimental cross-section ratio[41] for the $Ar^+(^2P_{1/2}, ^2P_{3/2})$ fine-structure branching ratio, which

strongly deviates from the statistical ratio 2 for both the $J=0$ and $J=2$ metastable states, Morgner[42] finds $u_{00}/u_{11}=-1/0.106$, which leads to a ratio $\Gamma_{\sigma'}(R)/\Gamma_{\pi'}(R)=|u_{00}/u_{11}|^2=89$ in our description. The relevant range of R values for Ne*[(3s)]-Ar ionizing collisions is determined by the range of classical turning points for trajectories with impact parameters $b \leq 6a_0$ (Fig. 3), resulting in a $6a_0 \leq R \leq 8a_0$ at collision energies of the order of $E \simeq 50$ meV. Figure 2 shows a ratio $\Gamma_{\sigma'}/\Gamma_{\pi'}=10.4$ increasing to 22.7 for R values increasing from $R=6a_0$ to $R=8a_0$, which implies an extra scaling factor between 8.6 and 3.9. With our simplified one-electron model, however, it is not possible to calculate the $Ar^+(^2P_{1/2},^2P_{3/2})$ fine-structure branching ratio.

Secondly, we can also determine this scaling factor by analyzing the Ne**[(3p);$J=3$]-Ar cross sections, with the ${}^3Q^{|M|=0}/{}^3Q^{|M|=3}$ ratio as the most sensitive parameter (Sec. VIII). This leads to a scaling factor 9 in favor of the σ' orientation. This factor is supported by the two-electron model calculations of the autoionization function for this system, as presented elsewhere,[44] which predict a scaling factor between 8 and 24 in the relevant range between $R=5a_0$ and $6a_0$.

As a compromise we have chosen the scaling factor equal to 9, which gives the best agreement with the available information for both the metastable Ne*(3s)-Ar and short-lived Ne**[(3p);$J=3$]-Ar systems. At $R=7a_0$ we then have a corrected ratio $\Gamma_{\sigma'}/\Gamma_{\pi'}=149$, slightly larger than derived from Morgner's analysis.[42]

We perform a semiclassical trajectory calculation for the Ne*[(3s);J]-Ar system, which will be described in further detail in Sec. VIII. Using the real potential $V(R)$ of Gregor and Siska[29] for both metastable states, we obtain a trajectory for all Ne*[(3s);JM]-states, independent of the quantum numbers J,M. The asymptotic magnetic substates of the Ne*[(3s);$J=2$] atom are considered to be space fixed along the classical trajectories because we neglect the Ω splitting for this system. Because the internuclear axis rotates during the collision, we apply the appropriate rotation matrix to calculate the changing Ω distribution along the trajectory. On a trajectory part $(\mathbf{R},\mathbf{R}+\Delta\mathbf{R})$ each Ω state moving with velocity v is attenuated by a factor $\exp[-\Gamma_{J\Omega}(R)\Delta R/(\hbar v)]$, with $\Gamma_{J\Omega}(R)$ given by Eq. (4). This factor represents the loss of flux of ionization.

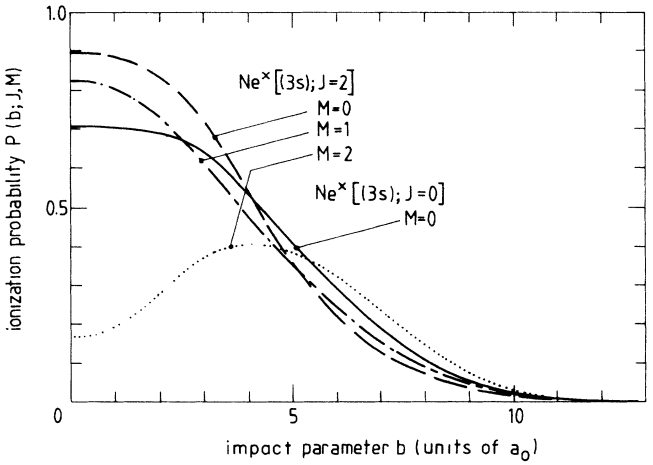

FIG. 3. The calculated ionization probability $P(b|J,M)$ for the asymptotic pure magnetic substates $|J,M\rangle_g$ of the metastable Ne*[(3s);$J=0,2$] states colliding with an Ar atom. Because the $|J=2,\Omega=2\rangle$ state ionizes very poorly, the $|J=2,M=\pm2\rangle_g$ has a small ionization probability for small impact parameters b. For large impact parameters the ionization probability becomes significant because a large $\Omega=0,1$ contribution is obtained due to rotational coupling. The $|J=2,M=0,\pm1\rangle_g$ states ionize poorly for large impact parameters, because rotational coupling results in a large $\Omega=2$ admixture. The Ne*[(3s);$J=0$]-Ar system has a significant ionization probability for all impact parameters which probe small internuclear distances.

For a trajectory with impact parameter b we obtain the ionization probability $P(b|J,M)$, which represents the fraction that is lost through ionization in a collision of an asymptotic magnetic substate $|J,M\rangle_g$. The total cross section for ionization ${}^JQ^{|M|}$ can be calculated by integrating the ionization probability $P(b|J,M)$ over the whole impact-parameter range according to

$$ {}^JQ^{|M|}=\int_0^\infty db\, 2\pi b P(b|J,M) \ . \tag{5}$$

For collision energies of $E=50$ and 100 meV we have performed a semiclassical calculation. In Table II we present the results for the isotropic cross sections ${}^0Q,{}^2Q$ and the polarization effect of ${}^2Q^{|M|}$. To compare the semiclassical results with experimental results, we have included experimental data of three authors in Table II. We observe a significant polarization effect in the ${}^2Q^{|M|}$ cross sections. Although the experimentally observed polarization effect of Bregel *et al.*[20] and Driessen *et al.*[21] is more pronounced, we conclude that the agreement is very good.

The Gregor and Siska potential[29] has been used as the real potential with no Ω splitting. Realistic potentials, however, have an Ω splitting in the real part as well (Sec. II A). In a second semiclassical calculation we use the suggested Ω splitting of Eq. (3). These calculated cross sections are also given in Table II. We observe a minor increase on the ratio ${}^0Q/{}^2Q$ and a slightly more significant polarization effect with respect to the previous calculation. The influence of the Ω splitting is very small because it is only probed at small impact parameters, which only give a minor contribution to the total cross section [Eq. (5)].

To understand the difference in the isotropic ionization cross sections ${}^0Q$ and ${}^2Q$, we have depicted the ionization probability $P(b|J,M)$ as a function of the impact parameter b in Fig. 3 for a collision energy $E=100$ meV. At this energy we probe internuclear distances $R>5.7a_0$, for which the σ' orientation has a much larger autoionization width $\Gamma_{\sigma'}(R)$ in comparison to the π' orientation (Fig. 1). Only those Ω states that contain a significant σ' contribution will be ionized. The Ne*[(3s);$J=0$] state has a constant σ' contribution $c_{\sigma'}(R)=\frac{1}{3}$, resulting in a significant ionized fraction $[P(b|J,M)>0.25]$ for a large impact-parameter range $0<b|a_0|<6.4$. In the case of a Ne*[(3s);$J=2$] state, only the $\Omega=0,1$ states have a σ'

TABLE II. Semiclassical results for the ionization cross section of the Ne*[(3s)]-Ar system without (1) and with (2) Ω splitting in the real potential $V(R)$, compared with experimental data of (a) Van den Berg *et al.*[43], (b) Bregel *et al.*[20], (c) Driessen *et al.*[21] The number in parentheses is the error in the last digit given.

	${}^0Q$ (Å^2)	${}^2Q$ (Å^2)	${}^0Q/{}^2Q$	Polarization effect ${}^2Q^0/{}^2Q$	${}^2Q^1/{}^2Q$	${}^2Q^2/{}^2Q$
$E=50$ meV						
Semiclassical						
(1)	19.7	17.9	1.10	1.07	1.04	0.93
(2)	19.7	17.9	1.10	1.08	1.04	0.92
Experiment						
(b)				1.13(3)	1.13(8)	0.81(3)
$E=100$ meV						
Semiclassical						
(1)	21.8	19.4	1.12	1.02	1.01	0.98
(2)	21.8	19.3	1.13	1.03	1.01	0.98
Experiment						
(a)	24.7	18.9	1.31			
(b)				1.07(4)	1.07(8)	0.89(4)
(c)				1.11(8)	1.11(8)	0.83(8)

contribution (Table I). The $\Omega=2$ state, however, has no σ' contribution and thus ionizes very poorly. This results in a significant ionized fraction $[P(b|J,M|>0.25]$ limited to those impact-parameter ranges, where a large $\Omega=0,1$ contribution is obtained at the turning point. As can be seen in Fig. 3, this impact-parameter range for the $\Omega=0$ state is $0<b(a_0)<5.7$; for the $\Omega=1$ state, $0<b(a_0)<5.9$; and for the $\Omega=2$ state, $1.7<b(a_0)<6.8$. The isotropic cross section for Ne*[(3s);$J=2$]-Ar, averaged for $M=-2$, is 12% smaller compared to the Ne*[(3s);$J=0$]-Ar cross section (Table II). This difference is fully accounted for by the nonlinear collision dynamics of the system. This supports our previous statement: Equal results for the spherical average of the autoionization width do not imply equal values of the ionization cross section for nonpolarized atoms. With decreasing ionization probability this effect becomes less important, resulting in a decrease of the calculated ratio to ${}^2Q/{}^0Q=1.05$ at $E=2500$ meV.[44] A small fine-structure dependence of the real part of the potential only modifies these values slightly.

Experimentally we find an increasing ratio, with ${}^0Q/{}^2Q=1.27$ at $E=75$ meV and ${}^0Q/{}^2Q=1.76$ at $E=2500$ meV.[38,46] Although a small contribution to the ratio ${}^0Q/{}^2Q$ is accounted for by these calculations, it is clear that so far no good explanation exists for the experimental magnitude and energy dependence of the ${}^0Q/{}^2Q$ ratio.

III. EXPERIMENTAL SETUP

The measurements have been performed in the crossed-beam apparatus, previously used by Verheijen *et al.*[38] and by Van den Berg, *et al.*[46] for state-selected measurements of the energy dependence of the ionization cross section of the Ne*[(3s);$J=0,2$]-(rare-gas, molecule) systems. A schematic view of the machine is given in Fig. 4, together with typical operating pressures in the differentially pumped vacuum chambers. In this section we only discuss the features that are important for the interpretation of the data. For the production of the metastable Ne* atoms two different discharge beam sources are available: a hollow cathode arc discharge (HCA) for the superthermal energy range $0.5<E$ (eV)<5 with a typical center line intensity $I(0)=10^{14}$ s^{-1}sr^{-1} and a discharge excited supersonic expansion (TMS) [$I(0)=2\times10^{13}$ s^{-1}sr^{-1}] for the thermal energy range $0.05<E$ (eV)<0.2. The sources can be interchanged rapidly without breaking the vacuum, which guarantees a good connection of measurements in the two different energy ranges. The primary beam is detected by Auger emission from an untreated stainless-steel surface, followed by a CuBe multiplier and pulse counting electron-

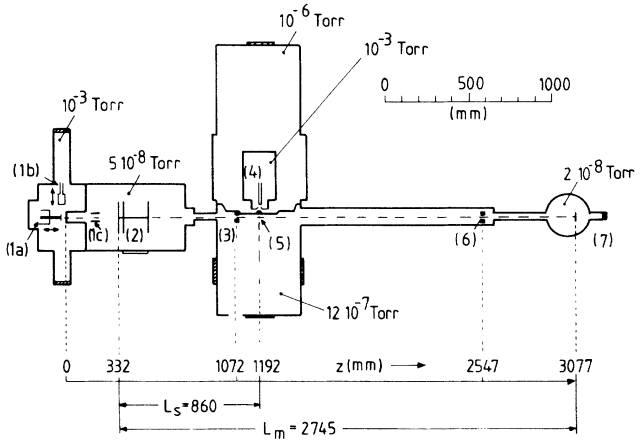

FIG. 4. Schematic view of the crossed-beam apparatus. The operating pressures in the different parts of the apparatus are indicated. (1) Metastable atom source: (1a) hollow cathode arc (HCA), (1b) thermal metastable source (TMS); (2) three-wheel time-of-flight (TOF) chopper; (3) collimator, 2 mm diameter; (4) supersonic secondary beam source; (5) scattering center; (6) collimator, 0.3 mm diameter; (7) metastable atom detector.

ics. The overall detection efficiency of the system is $\eta^m=0.54$, which is determined relative to the ion detection efficiency $\eta^{ion}=0.60$ in the scattering center by using the Ne*[(3*s*);*J*=2]-Ar ionization cross section $^2Q=18.3$ Å^2 at $E=0.1$ eV (Ref. 46) as a calibration factor. Velocity analysis is performed with a single-burst time-of-flight method, using a mechanical chopper. The chopper disc has two slits of different width, which allows us to choose a time resolution appropriate for each beam source. The open time can be chosen as 0.67% or 2% of the chopper period. The flight path between the first chopper disc and the metastable atom detector is $L_d=2747$ mm. The primary beam is collimated 870 mm downstream of the beam source with a 2-mm-diam circular orifice, resulting in a time-averaged flux of 10^8 s^{-1} or 5×10^8 s^{-1} metastable atoms in the scattering center.

A single-mode Spectra Physics 580A cw dye laser is applied for optical pumping of the Ne*[(3*s*);*J*=2] $\leftrightarrow$Ne**[(3*p*);*J*=3] closed-level system at $\lambda=640.2$ nm. The laser beam can reach the scattering center from two directions: perpendicular to the collision plane defined by the beam velocities $\mathbf{v}_1$ and $\mathbf{v}_2$ or antiparallel to the secondary beam velocity $\mathbf{v}_2$. The former configuration is used for both linear and circular polarized light; the latter is only used for a circular polarization. The size of the laser beam at the scattering center is 3.6 mm full width at $1/e^2$ of maximum intensity. The laser beam and the primary beam are always at right angles, with an accuracy of 0.2 mrad as obtained by an automated procedure.[47]

In the scattering center the primary beam is crossed at right angles with a supersonic secondary beam. This system is double differentially pumped with a slit skimmer and a rectangular collimator (2×5 mm^2) as beam limiting devices, resulting in a well-defined and narrow beam profile over the cross section of the primary beam. The width of this profile, i.e., the scattering length of the primary beam atoms, is equal to 2.35 mm at 50% of the maximum beam density and 2.8 mm at 10% of the maximum density. Compared to the full width waist of the laser beam (3.6 mm), this guarantees an excellent overlap of the laser beam with the beam profile. The density-length product $\langle nl\rangle$ has been calibrated by Verheijen *et al.*[48] for the rare gases Ar, Kr, and Xe, resulting in $\langle nl\rangle=2.8\times10^{15}$ m^{-2}, 2.2×10^{15} m^{-2}, and 1.8×10^{15} m^{-2}, respectively, for a reservoir pressure of 120 Torr. The resolution in the collision energy E is determined mainly by the time-of-flight spectrum of the ions, due to this shorter flight path. Typical values are $\Delta v_1/v_1=4.5\%$ at $v_1=1000$ ms^{-1} and $\Delta v_1/v_1=12\%$ at $v_1=7500$ ms^{-1}, resulting in an energy resolution $\Delta E/E=7.5\%$ at $E=80$ meV in the thermal energy range and $\Delta E/E=24\%$ at $E=4.5$ eV in the superthermal energy range.

IV. OPTICAL PUMPING

A. Upper-level population

In order to analyze the measured data in terms of the ionization cross section, we have to know the upper-level population density in the interaction region. The relative population η^{opt} of the upper level is determined by absorption, stimulated emission, and spontaneous emission. For low laser intensities I spontaneous emission is dominant over stimulated emission and an equal population distribution cannot be reached ($\eta^{opt}<\frac{1}{2}$). In the case of large laser intensities I stimulated emission is dominant and equal populations in the two-level system will be reached ($\eta^{opt}=\frac{1}{2}$). The relative population η^{opt} of the upper level is a function of the laser intensity I, as given by[49]

$$\eta^{opt}=\tfrac{1}{2}\frac{(I/I_s)}{1+(I/I_s)}\ , \tag{6}$$

with I_s the saturated laser intensity at $\eta^{opt}=\frac{1}{4}$. We have measured the ion signal with the excited two-level system in the scattering center as a function of the laser intensity I. If the difference in ionization cross section of the upper and the lower level is large, the ion signal will show a large dependence on the laser intensity I. This requirement is met in the Ne*(*)-H_2 system.[50,51] In Fig. 5 we show the experimental results of the ratio $\mathcal{R}$ of the ion signals with laser on and off, as a function of the laser intensity, together with a least-squares analysis with the model function of Eq. (6). The result for the saturated laser intensity is $I_s=120$ μW/mm^2, which is a factor 3 larger than the theoretical value.[49] In our analysis of Eq. (6) we neglected the Gaussian laser beam profile (3.6 mm at $1/e^2$ intensity) overlapping the secondary beam profile (2.8 mm at $\frac{1}{10}$ density). The ion signal from the edges of the scattering center saturates at larger laser intensities I, leading to a larger effective value of I_s in our analysis. The ionization cross-section measurements with the two-level system have been performed at laser intensities in the range $6<I/I_s<11$, with a corresponding range

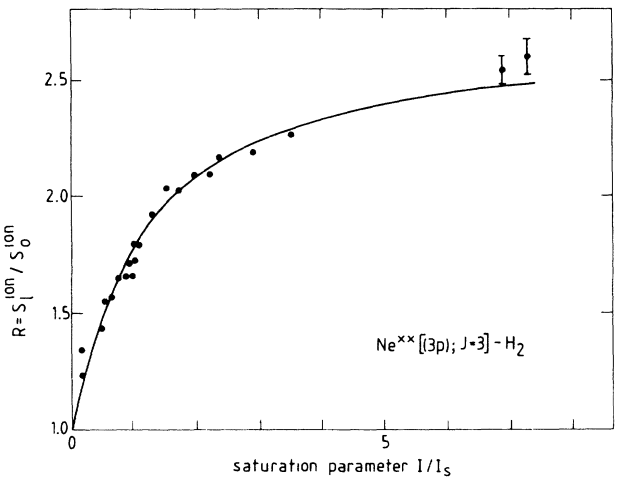

FIG. 5. The ratio $\mathcal{R}$ of the ion signals with laser on and off, respectively, for the Ne**-H_2 system as a function of the laser intensity I, for a linear laser polarization and $\beta=\pi/4$. The least-squares analysis of the data with the model function of Eq. (6) is given by the solid line. All $\Delta Q(E)$ measurements have been performed in the laser intensity region $6<I/I_s<11$.

TABLE III. Asymptotic populations $g^{|M|}(\beta)$ and the alignment parameter A [Eq. (7)] for the $Ne^*[(3s);J=2]$ and the $Ne^{**}[(3p);J=3]$ atoms, polarized by optical pumping with four linear laser polarizations [$\beta=\angle(\mathbf{E},\mathbf{g})$] and a circular laser polarization [$\beta=\angle(\mathbf{k},\mathbf{g})$].

	$Ne^*[(3s);J=2]$				$Ne^{**}[(3p);J=3]$				
	$g^0(\beta)$	$g^1(\beta)$	$g^2(\beta)$	A	$g^0(\beta)$	$g^1(\beta)$	$g^2(\beta)$	$g^3(\beta)$	A
$\angle(\mathbf{E},\mathbf{g})$									
$\beta=0$	0.476	0.476	0.048	-4	0.476	0.476	0.048	0.000	-10
$\beta=\pi/6$	0.321	0.516	0.163	$-2\frac{1}{2}$	0.223	0.468	0.266	0.043	$-6\frac{1}{4}$
$\beta=2\pi/6$	0.151	0.409	0.440	$\frac{1}{2}$	0.108	0.217	0.375	0.300	$1\frac{1}{4}$
$\beta=3\pi/6$	0.137	0.262	0.601	2	0.089	0.208	0.173	0.530	5
$\angle(\mathbf{k},\mathbf{g})$									
$\beta=\pi/2$	0.375	0.500	0.125	-3	0.312	0.469	0.188	0.031	$-7\frac{1}{2}$

$0.43<\eta^{\text{opt}}<0.46$ for the upper-level population. In the data analysis we will use the average value $\eta^{\text{opt}}=0.45$ for all velocities of the primary beam and for all different series. This only introduces a minor correction of the order of a few percent. Of course, it could be corrected for in each series.

B. Degree of polarization

Repeated excitation of the two-level system $Ne^*[(3s);J=3]\leftrightarrow Ne^{**}[(3p);J=3]$ with a polarized laser beam results in a beam of polarized atoms with a stationary distribution over the magnetic substates. For a linear polarized laser beam the natural quantization axis is the electric field vector $\mathbf{E}$; for a circular polarization the wave vector $\mathbf{k}$ serves this purpose. The polarized atom is most conveniently characterized by the relative population $g^M(0)$ of the magnetic substates with respect to this axis. The stationary values are determined by the relative transition probabilities within the two-level system. The degree of polarization can also be characterized by the parameter A as given by[52,53]

$$A=\sum_{M=-J}^{+J}[3M^2-J(J+1)]g^M(0)/\sum_{M=-J}^{+J}g^M(0)\ . \tag{7}$$

For the scattering process of the polarized atoms the relative velocity $\mathbf{g}$ is the relevant quantization axis. The relative populations $g^M(\beta)$ of the magnetic substate $|J,M\rangle$ with respect to this axis are given by

$$g^M(\beta)=\sum_{M'=-J}^{+J}[d^J_{MM'}(\beta)]^2 g^{M'}(0)\ , \tag{8}$$

with β the angle between the optical quantization axis ($\mathbf{E}$ or $\mathbf{k}$) and the relative velocity $\mathbf{g}$. The Wigner d function $d^J_{MM'}(\beta)$ describes the M' mixing due to the quantum-mechanical rotation operator. Because coherence effects do not contribute to the total ionization cross section (Sec. V A), the rotation operator $\mathcal{D}^J_{MM'}(\alpha,\beta,\gamma)$ over the Euler angles is replaced by the Wigner d function that takes on real values only.

In Table III we present the relative populations $g^{|M|}(\beta)$ of the $|J,M\rangle$ states ($g^{|M|}=g^{+M}+g^{-M}$, $M\neq 0$) for five experimental laser configurations. In case of a linear laser polarization we get a broad $|M|$ distribution at $\beta=0$. Although we can match the relevant quantization axes $\mathbf{E}$ and $\mathbf{g}$, no pure magnetic substate with respect to $\mathbf{g}$ can be excited. In case of a circular laser polarization a pure magnetic substate is excited with respect to the wave vector $\mathbf{k}$, resulting in $g^3(0)=1$. It is impossible, however, to match this optical quantization axis $\mathbf{k}$ with the collisional quantization axis $\mathbf{g}$, because this results in an unacceptable Doppler shift with respect to the primary beam velocity $\mathbf{v}_1$. Thus, for all possible laser polarizations we will get a linear combination of magnetic substates with respect to the relative velocity $\mathbf{g}$.

Using a computer simulation involving a Gaussian laser beam profile, we have calculated the number of absorption–spontaneous-emission cycles that is necessary to obtain an A value equal to 90% of its stationary value. For a linear polarized laser beam this number is eight excitations. For a right-handed (RHC) of left-handed (LHC) circularly polarized beam a larger number of 20 excitations is necessary to meet this condition. For this latter case the stationary distribution represents a two-level system $Ne^*[(3s);|J=2,M=\pm 2\rangle_k]\leftrightarrow Ne^{**}[(3p);|J=3,M=\pm 3\rangle_k]$ with the + sign for RHC and the − sign for LHC. In our case the beam profile of the secondary beam (2.8 mm at $\frac{1}{10}$ density) is located well within the laser beam profile (3.6 mm at $1/e^2$ intensity). The primary beam particles have reached 90% of its stationary M distribution before entering the secondary beam profile.

V. CROSS-SECTION MEASUREMENTS

A. Polarized-atom cross sections

For the scattering process of the polarized atoms the relative velocity $\mathbf{g}$ is the relevant quantization axis. The relative populations $g^M(\beta)$ of the magnetic substate $|J,M\rangle$ with respect to this axis are given by Eq. (8). The effective ionization cross section ${}^JQ(\beta)$ for this beam of polarized atoms is then a linear combination of pure-state ionization cross section ${}^JQ^{|M|}$ with the relative velocity as the quantization axis, as given by

$${}^JQ(\beta)=\sum_{M=-J}^{+J}g^M(\beta){}^JQ^{|M|}\ . \tag{9}$$

Of course, the ionization cross section also depends on the collision energy E. For a given experimental situa-

tion the direction of the relative velocity **g** will depend on the collision energy E, and thus β will also depend on **g** and thus on E.

The cross section ${}^{J}Q(\beta)$ does not include coherence effects between the different $|J,M\rangle_g$ states. If the total cross section is measured for a collision involving *one* polarized atom, there is cylinder symmetry with respect to **g**. The result is thus invariant for a rotation over an angle φ about this axis. Coherence effects, however, are proportional to a phase factor $\exp[-i(M-M')\varphi]$. The integration over all impact parameters contains an integration over the angle φ from 0 to 2π canceling the coherence terms for $M \neq M'$. Coherence effects thus do not influence ${}^{J}Q(\beta)$. In collisions of *two* polarized atoms there is no cylindrical symmetry about the relative velocity **g**. Therefore coherence effects will contribute to the total cross section, as has been observed by Meijer *et al.*[7] in collisions of two $Na^*(3p)$ atoms.

For a nonpolarized atom the weight factors are equal to the statistical weights $g^M=(2J+1)^{-1}$, resulting in the correct expression for the isotropic ionization cross section

$$ {}^{J}Q=(2J+1)^{-1}\sum_{M=-J}^{+J} {}^{J}Q^{|M|} , \tag{10}$$

which is measured, e.g., in a bulk experiment without any information on the orientation of the relative velocity **g** of the colliding particles.

B. Experimental signals

The time-of-flight spectrum of the primary beam of metastable Ne* atoms is measured downstream of the scattering center, using a flight path L_d from chopper to detector. For each chopper period the number of counts $S^m(t_n|L_d)$ measured in time channel n centered at flight time $t_n=L_d/v_n$, with v_n the velocity of the atom, is given by

$$\begin{aligned} S^m(t_n|L_d) &= \eta^m I(0)\Omega_d F(t_n|L_d)\tau_{\rm ch} \\ &= \eta^m \dot{N}^m(t_n|L_d)\tau_{\rm ch} , \end{aligned} \tag{11}$$

with η^m the efficiency for metastable-atom detection. The flux $\dot{N}^m(t_n|L_d)$ of metastable atoms arriving at the detector with flight time t_n is determined by the center line intensity $I(0)$ ($s^{-1}sr^{-1}$), the solid angle Ω_d of the primary beam seen by the detector, the duration of one time channel $\tau_{\rm ch}$, and the flight-time distribution $F(t_n|L_d)$. From the time-of-flight spectrum $S^m(t_n|L_d)$ we can determine by deconvolution the velocity distribution, which is then convoluted once more to determine the time-of-flight spectrum $S^m(t_k)$ of metastable atoms arriving at the scattering center. This procedure of spectrum transformation is described in detail by Van Vliembergen *et al.*[54]

The beam of metastable atoms has an isotropic distribution $^{20}Ne:{}^{21}Ne:{}^{22}Ne=90.9:0.3:8.8$ and for each isotope a distribution over the two metastable states. For Ne* the latter is always close to the ratio $Ne^*[(3s);J=2]:Ne^*[(3s);J=0]=5:1$ determined by the statistical weights. For the production of atoms in the short-lived upper level, we are only interested in the rate of arrival ${}^{2}\dot{N}(t_k)$ of the metastable $^{20}Ne^*[(3s);J=2]$ atoms. However, information has to be extracted from the time-of-flight spectrum $S^m(t_k)$ of all metastable atoms. This requires a careful analysis of all assumptions entering the analysis. First we have to consider the detection efficiencies for both metastable states. The time-of-flight spectrum $S^m(t_k)$ has to be written as

$$S^m(t_k)={}^{2}\eta^m\,{}^{2}\dot{N}(t_k)\tau_{\rm ch}+{}^{0}\eta^m\,{}^{0}\dot{N}(t_k)\tau_{\rm ch}+{}^{r}\eta^m\,{}^{r}\dot{N}(t_k)\tau_{\rm ch} , \tag{12}$$

where the superscript indicating the metastable states with $J=2$ and $J=0$, respectively, or the metastable isotopes, indicated by the superscripts r. Although there is some experimental evidence for a different detection efficiency for both metastable states, we assume throughout this paper that $\eta^m={}^{0}\eta^m={}^{2}\eta^m={}^{r}\eta^m$. Second, we have to consider the shape of the flight-time distributions for the different species. Due to the larger mass of the ^{22}Ne isotopes, we can expect that in a supersonic expansion these atoms will lag behind, usually indicated by slip. In a separate experiment[55] this effect has been studied resulting in a flow velocity ratio for the two isotopic species of $u(^{22}Ne)/u(^{20}Ne)=0.98$. This small effect has been neglected. The approximation used for the rate of arrival of $^{20}Ne^*[(3s);J=2]$ atoms at the scattering center is then given by

$${}^{2}\dot{N}(t_k)={}^{2}f\dot{N}^m(t_k)={}^{2}fS^m(t_k)/(\eta^m\tau_{\rm ch}) , \tag{13}$$

with ${}^{2}f$ the relative population of the $^{20}Ne^*[(3s);J=2]$ atoms. We get similar expressions for the other metastable state ${}^{0}\dot{N}(t_k)={}^{0}f\dot{N}^m(t_k)$ and for the ^{22}Ne isotope ${}^{r}\dot{N}(t_k)={}^{r}f\dot{N}^m(t_k)$. Assuming a statistical distribution over the two metastable states we get ${}^{2}f=0.7575$, ${}^{0}f=0.1515$, and ${}^{r}f=0.091$. With the laser beam switched on, the rate of arrival of atoms in the short-lived upper level is then equal to ${}^{3}\dot{N}(t_k)=\eta^{\rm opt}\,{}^{2}\dot{N}(t_k)$.

Collisions with secondary beam atoms at the scattering center will produce ions. The number of counts from the spiraltron $S_0^{\rm ion}(t_k)$ that is registered in time channel k of each chopper period is equal to

$$\begin{aligned} S_0^{\rm ion}(t_k) &= \eta^{\rm ion}\tau_{\rm ch}\langle(g_k/v_k)nl\rangle\dot{N}^m(t_k) \\ &\quad\times[{}^{2}f\,{}^{2}Q(g_k)+{}^{0}f\,{}^{0}Q(g_k)+{}^{r}f\,{}^{r}Q(g_k)] , \end{aligned} \tag{14}$$

with $\langle(g_k/v_k)nl\rangle$ the effective density-length product of the secondary beam, including the kinematic factor g_k/v_k. This expression is valid when the attenuation of the primary beam by elastic collisions is small.[38] We assume that the cross section of the ^{22}Ne isotope, denoted as ${}^{r}Q$, is equal to that of the ^{20}Ne isotope. Without the laser beam the atoms are unpolarized. In this situation we measure a cross section that is weighted with the statistical populations $({}^{0}Q+5\,{}^{2}Q)/6$. Switching on the laser results in a decrease of the ${}^{2}\dot{N}(t_k)$ signal and a corresponding increase of the upper-level signal, resulting in

$$S_{\gamma}^{\text{ion}}(t_k|\beta_k)=\eta^{\text{ion}}\tau_{\text{ch}}\langle(g_k/v_k)nl\rangle\dot{N}^m(t_k)\times[\eta^{\text{opt}\,2}f^3Q(g_k|\beta_k)+(1-\eta^{\text{opt}})^2f^2Q(g_k|\beta_k)+{}^0f\,{}^0Q(g_k)+{}^rf\,{}^rQ(g_k)]\ . \quad (15)$$

Both the upper and the lower level become polarized and we have to use the effective polarized-atom cross sections ${}^JQ(g_k|\beta_k)$ to calculate the contribution to the ion signal. The direction of the relative velocity $\mathbf{g_k}$ in the Newton diagram depends on the magnitude of the primary beam velocity $\mathbf{v_k}$, which implies that at a fixed laser polarization the angle β also depends on the time channel k. The difference of the ion signals with laser switched "on" and "off" is given by

$$\Delta S^{\text{ion}}(t_k|\beta_k)=S_{\gamma}^{\text{ion}}(t_k|\beta_k)-S_0^{\text{ion}}(t_k)=\eta^{\text{ion}}\tau_{\text{ch}}\langle(g_k/v_k)nl\rangle\dot{N}^m(t_k)\times\{\eta^{\text{opt}\,2}f[{}^3Q(g_k|\beta_k)-{}^2Q(g_k|\beta_k)]+{}^2f[{}^2Q(g_k|\beta_k)-{}^2Q(g_k)]\}\ . \quad (16)$$

This equation shows that for the analysis of the polarized-atom cross section of the upper level we need both the isotropic cross section ${}^2Q(g)$ as well as the effective polarized-atom cross section ${}^2Q(g|\beta)$ of the lower metastable state Ne*[(3s);$J=2$].

The final result for the effective cross-section difference $\Delta Q(g_k|\beta_k)$ is

$$\Delta Q(g_k|\beta_k)={}^3Q(g_k|\beta_k)-{}^2Q(g_k|\beta_k)=(\eta^{\text{opt}})^{-1}[{}^2Q(g_k|\beta_k)-{}^2Q(g_k)]+\langle(g_k/v_k)nl\rangle^{-1}(\eta^{\text{opt}})^{-1}\times\frac{\Delta S^{\text{ion}}(t_k|\beta_k)}{{}^2fS^m(t_k)}\frac{\eta^m}{\eta^{\text{ion}}}\ . \quad (17)$$

This result can be used to determine $\Delta Q(g_k|\beta_k)$ from the experimental signals. Two types of measurements have been performed. First, the ion signal difference has been measured as a function of β without velocity selection (Sec. VI). Second, at five angles β_k, the time-of-flight spectra have been measured and analyzed in terms of the energy dependence of the polarized-atom cross section (Sec. VII).

VI. POLARIZATION EFFECTS IN ${}^3Q(\beta)$

A. Experimental procedure

As we already discussed in Sec. IV B, it is not possible in our experimental setup to excite a pure magnetic substate $|J=3,M\rangle$ with respect to the relative velocity $\mathbf{g}$. Therefore, the polarized cross section ${}^3Q(\beta)$ will be measured for several independent laser polarizations. Solving the system of linear equations in Eq. (9) will result in the polarized cross sections ${}^3Q^{|M|}$.

To obtain a high accuracy in the polarization effect, we have first sacrificed the energy resolution. Without the time-of-flight chopper very large ion signals are obtained. The cross sections resulting from these signals are average values at the collision energy of the two atomic-beam sources available. The ratio $\mathcal{R}(\beta)$ of the ion signal with laser on and off [Eqs. (14) and (15)] can be written as

$$\mathcal{R}(\beta)=\frac{S_{\gamma}^{\text{ion}}(\beta)}{S_0^{\text{ion}}}=1+\frac{\eta^{\text{opt}\,2}f[{}^3Q(\beta)-{}^2Q(\beta)]+{}^2f[{}^2Q(\beta)-{}^2Q]}{{}^2f\,{}^2Q+{}^0f\,{}^0Q+{}^rf\,{}^rQ}\ . \quad (18)$$

The polarized-atom cross sections ${}^3Q(\beta)$ and ${}^2Q(\beta)$ have a β dependence according to Eqs. (8) and (9). If we neglect the polarization effect for the metastable lower level [${}^2Q(\beta)={}^2Q={}^2Q^{|M|}$], this ratio can be simplified to

$$\mathcal{R}(\beta)=1+\frac{\eta^{\text{opt}\,2}f[{}^3Q(\beta)-{}^2Q]}{{}^2f\,{}^2Q+{}^0f\,{}^0Q+{}^rf\,{}^rQ}\ . \quad (19)$$

With the exception of the polarized-atom cross sections ${}^3Q^{|M|}$ of the Ne**[(3p);$J=3$] state, all the parameters in this equation are known. The relative populations ${}^0f$, ${}^2f$, and ${}^rf$ are given in Sec. V B. Cross-section values for the two metastable states are obtained from state-selective measurements by Verheijen *et al.*[38] The relative population η^{opt} of the upper level has been fixed at $\eta^{\text{opt}}=0.45$ (Sec. IV A).

We measure the ion signals with laser on and off, as a function of the angle β between the laser quantization axis $\mathbf{E}$ and the relative velocity $\mathbf{g}$, by rotating the linear laser polarization $\mathbf{E}$ in the collision plane $(\mathbf{v}_1,\mathbf{v}_2)$. Extreme values are obtained for $\beta=0$ and $\beta=\pi/2$. The polarized-atom cross sections ${}^3Q^{|M|}$ can be determined by performing a least-squares analysis of the experimental results for $\mathcal{R}(\beta)$.

B. Experimental results

The ratio $\mathcal{R}(\beta)$ of the ion signals with laser on and off has been measured for the Ne*(**)-Ar,Kr,Xe systems. With the two primary beam sources we obtain β-dependent results for two collision energies ($E=130\pm50$ meV and $E=2.5\pm1.5$ eV). The experimental results for $\mathcal{R}(\beta)$ for the Ne*(**)-Ar system are depicted in Fig. 6. For the Ne*(**)-Kr, Xe systems the results are quite similar. We observe a significant polarization effect in the thermal energy range for all systems [$I_{\max}/I_{\min}\approx1.15$], whereas in the superthermal energy range the polarization effect barely exceeds the statistical error bars ($I_{\max}/I_{\min}\approx1.01$).

Based on the $J=3$ symmetry of the upper level, the ratio $\mathcal{R}(\beta)$ can be written as

$$\mathcal{R}(\beta)=\sum_{n=0}^{3}R_n\cos(2n\beta)\ , \quad (20)$$

where the R_n coefficients can be interpreted in ${}^3Q^{|M|}$ cross sections according to Eq. (19). In a least-squares analysis of the data, the coefficients R_2 and R_3 were found to be negligible for all systems, resulting in

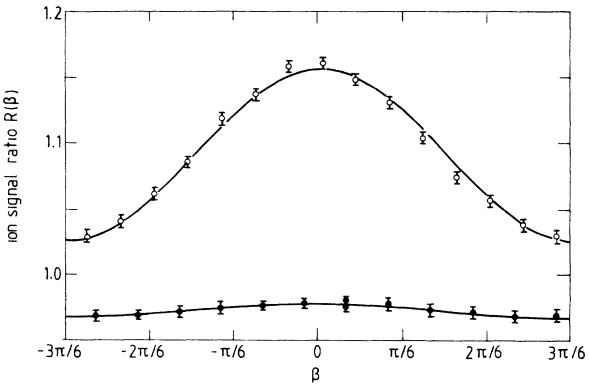

FIG. 6. Experimental results for the ratio $\mathcal{R}(\beta)$ for the Ne**[(3p);J=3]-Ar system as a function of the angle β obtained without energy resolution. Using the two primary beam sources, we obtain results for two average energies $E=130\pm50$ meV (open symbols) and $E=2500\pm1500$ meV (solid symbols).

${}^3Q^2={}^3Q$. The coefficients R_0 and R_1 are given in Table IV. The polarized-atom cross sections ${}^3Q^{|M|}$ which are obtained from these coefficients using Eq. (19) are given in Table IV as well, together with the state-selected cross sections ${}^0Q$ and ${}^2Q$ of the two metastable states that are needed in the analysis. The polarization effect for Ne**[(3p);J=3]-Ar in the thermal energy range agrees well with the experimental results of Bussert *et al.*,[5] which have also been included in Table IV. In the thermal energy range the polarized-atom cross sections ${}^3Q^{|M|}$ differ by a factor of 2. The asymptotic $|J=3,M=0\rangle_g$ state has the largest cross section; the smallest cross section is observed for the $|J=3,M=\pm3\rangle_g$ states. The cross sections ${}^3Q^0$ and ${}^3Q^1$ have large error bars because the $|M|=0,1$ states are almost equally populated for every angle β (Table III). The ${}^3Q^3$ cross section, however, can be solved very accurately because the population of the $|M|=3$ state varies appreciably with respect to the other $|M|$ states as a function of the angle β. In this analysis we neglected the polarization effect of the Ne*[(3s);$J=2,M$] lower level. In the Sec. VII with the time-of-flight results we will take into account this lower-level polarization effect in a second analysis.

VII. ENERGY DEPENDENCE OF POLARIZED-ATOM CROSS SECTIONS ${}^3Q^{|M|}$

A. Experimental procedure

Six different laser polarizations are chosen for which time-of-flight experiments are performed: four linear and two circular laser polarizations based on the $\mathcal{R}(\beta)$ measurements of Sec. VI. In the thermal energy range extreme values for $\mathcal{R}(\beta)$ are obtained for laser polarizations $\mathbf{E}\|\langle\mathbf{g}\rangle$ and $\mathbf{E}\perp\langle\mathbf{g}\rangle$, with $\langle\mathbf{g}\rangle$ the average relative velocity in this energy range. The four linear laser polarizations are chosen with respect to these orientations, making angles of $\angle(\mathbf{E},\langle\mathbf{g}\rangle)=0$, $\pi/6$, $\pi/3$, and $\pi/2$. As can be seen in Fig. 7, this results in angles $\angle(\mathbf{E},\mathbf{g_k})=\beta_0+i\pi/6$ (i=0,1,2,3) for the time-of-flight measurements with $\beta_0\approx0$ in the thermal energy range and $\beta_0\approx\pi/6$ in the superthermal energy range. Two circular laser polarizations are chosen, one with the wave vector $\mathbf{k}$ perpendicular to the collision plane [$\beta=\angle(\mathbf{k},\mathbf{g_k})=\pi/2$] and one with $\mathbf{k}$ antiparallel to the secondary beam velocity $\mathbf{v}_2$ [$\beta=\angle(\mathbf{k},\mathbf{g}_k)=\arctan(v_k/v_2)$]. In the latter case this results in an angle $\beta\approx\pi/3$ in the thermal energy range and $\beta\approx\pi/2$ in the superthermal energy range. From a Newton diagram the angle β_k between the optical quantization axis ($\mathbf{E}$ or $\mathbf{k}$) and the relative velocity $\mathbf{g_k}$ for time channel k of the time-of-flight spectrum can be determined (Fig. 7). Assuming a stationary M distribution with respect to the optical quantization axis, we use Eq. (6) to calculate the M distribution of both upper and lower level with respect to the radiative velocity $\mathbf{g_k}$.

TABLE IV. The R_0 and R_1 coefficients for Ne*(**)-Ar,Kr,Xe in two energy ranges: (I) $E=130\pm50$ meV, (II) $E=2.5\pm1.5$ eV. Using the isotropic cross sections ${}^0Q$ and ${}^2Q$ we obtain the polarized-atom cross sections ${}^3Q^{|M|}$. The ${}^3Q^{|M|}$ values are scaled with the isotropic cross section ${}^3Q$ to show the polarization effect more clearly.

	R_0	R_1	${}^0Q$ (Å^2)	${}^2Q$ (Å^2)	${}^3Q$ (Å^2)	${}^3Q^{\|M\|}/{}^3Q$ $\|M\|=0$	$\|M\|=1$	$\|M\|=2$	$\|M\|=3$
				$E=130\pm50$ meV					
Ar	1.092(4)	0.065(2)	22.3	17.2	20.9	1.26(3)	1.20(3)	1.00(2)	0.67(1)
Kr	1.073(5)	0.071(2)	21.2	14.5	16.7	1.31(4)	1.23(4)	1.00(3)	0.62(1)
Xe	1.153(8)	0.075(4)	15.1	12.2	16.9	1.26(6)	1.19(5)	1.00(3)	0.68(2)
				$E=2.5\pm1.5$ eV					
Ar	0.972(7)	0.005(3)	34.7	20.1	18.2	1.03(6)	1.02(6)	1.00(4)	0.96(2)
Kr	0.968(9)	0.005(3)	34.8	16.8	14.9	1.03(7)	1.02(7)	1.00(4)	0.96(2)
Xe	0.975(9)	0.009(3)	28.2	13.9	12.2	1.05(9)	1.04(8)	1.00(5)	0.94(3)
Ar	Bussert *et al.*[a]			$E=30\pm10$ meV		1.25(9)	1.19(7)	1.00(9)	0.68(7)
Ar	Bussert *et al.*[a]			$E=55\pm20$ meV		1.31(9)	1.23(7)	1.00(9)	0.61(7)
Ar	Bussert *et al.*[a]			$E=110\pm30$ meV		1.39(9)	1.28(7)	1.00(9)	0.51(7)

[a]References 5 and 27.

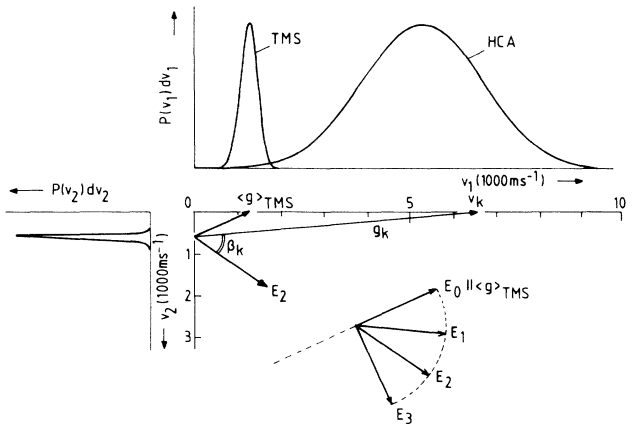

FIG. 7. The Newton diagram of the colliding particles. The average relative velocity $\langle \mathbf{g} \rangle$ in the thermal energy range has been indicated. The linear laser polarizations $\mathbf{E}_i$ for the time-of-flight measurements have been selected with respect to this velocity $\langle \mathbf{g} \rangle$. The angle $\beta_k = \angle(\mathbf{E}_i, \mathbf{g}_k) = \beta_0 + i\pi/6$ can be determined from this Newton diagram.

As mentioned in Sec. V B, we measure the metastable-atom signal [Eq. (11)] and the difference of the ion signals with the laser switched on and off [Eq. (16)]. The final result for the effective polarized-atom cross-section difference $\Delta Q(g_k|\beta_k)$ of Eq. (17) can be rewritten, giving the effective ionization cross section

$$^3Q(g_k|\beta_k) = {}^2Q(g_k|\beta_k) + \Delta Q(g_k|\beta_k) \tag{21}$$

for the upper level. The ionization cross section $^2Q(g_k)$ has been determined in state-selective measurements.[38] If we neglect the polarization effect in the lower-level cross section $^2Q(g_k)$, we can write the effective cross section $^3Q(g_k|\beta_k)$ of the upper level as

$$\begin{aligned} ^3Q(g_k|\beta_k) &= {}^2Q(g_k) + \Delta Q(g_k|\beta_k) \\ &= {}^2Q(g_k) + \langle (g_k/v_k) nl \rangle^{-1} (\eta^{\text{opt}})^{-1} \\ &\quad \times \frac{\Delta S^{\text{ion}}(t_k|\beta_k)}{{}^2fS^M(t_k)} \frac{\eta^m}{\eta^{\text{ion}}} . \end{aligned} \tag{22}$$

The first term for $\Delta Q(g_k|\beta_k)$ in Eq. (17) is then equal to zero and does not contribute to Eq. (22). Using the results of the time-of-flight measurements for the six laser polarizations, it is possible to determine the polarized-atom cross sections $^3Q^{|M|}(g_k)$ by performing a least-squares analysis of the six experimental $^3Q(g_k|\beta_k)$ values with the model function of Eq. (22).

To determine the influence of the polarization effect of the lower level on the polarized-atom cross sections $^3Q^{|M|}(g_k)$, we performed a second least-squares analysis of the data with Eq. (21). Only scarce experimental data are available for the $^2Q^{|M|}(g_k)$ polarization effect of the Ne*-Ar system [Table II]. The preliminary results of Driessen[21] have been obtained by optical depletion of single magnetic substates in a magnetic field **B**. These data indicate an energy-independent polarization effect for the Ne*-Ar system of $^2Q^0(g_k):{}^2Q^1(g_k):{}^2Q^2(g_k) = 4:4:3$.

B. Experimental results

For the least-squares analysis of the polarized-atom cross sections we have to determine the M distributions for the various laser configurations. In none of the prepared laser configurations is it possible to obtain a pure magnetic substate with respect to the relative velocity **g** (Sec. IV B). In Table III the M distributions are given for five independent laser polarizations. These results show that the $|J=3, M=0\rangle_g$ and the $|J=3, M=\pm 1\rangle_g$ states are almost equally populated for all laser configurations used and it is hardly possible to discern between the two polarized-atom cross sections $^3Q^0(g_k)$ and $^3Q^1(g_k)$ [Sec. VI B]. Therefore we assume these cross sections to be equal, leaving three polarized-atom cross sections $^3Q^{|M|}(g_k)$ to be determined in our least-squares analysis of Eqs. (21) and (22) with $^3Q^0(g_k) = {}^3Q^1(g_k)$, $^3Q^2(g_k)$, and $^3Q^3(g_k)$ as free parameters.

In Fig. 8 we present the isotropic ionization cross sections $^3Q(E)$ and $^2Q(E)$ as a function of the collision energy E, for the two $Ne^{*(*)}$ states of the two-level system colliding with Ar, Kr, and Xe. Using Chebyshev polynomials[56] $T_k(x)$ $(-1 < x < 1)$, we have performed a least-squares analysis of the isotropic cross sections $^3Q(E)$ and $^2Q(E)$ in the energy range $0.05 < E\,(\text{eV}) < 5$ according to

$$^JQ(E) = \sum_{k=0}^{n} c_k T_k[x = \log_{10}(E/0.5\ \text{eV})] . \tag{23}$$

The coefficients c_k of this analysis are given in Table V. We observe a similar energy dependence for all three rare

TABLE V. The c_k coefficients obtained with a least-squares analysis of the isotropic cross sections $^2Q(E)$ and $^3Q(E)$ according to Eq. (23) for the $Ne^{*(*)}$-(Ar,Kr,Xe) systems.

		c_k coefficients (Å^2)					
		c_0	c_1	c_2	c_3	c_4	c_5
^2Q	Ar	18.16	−1.44	−4.27	−1.52	0.74	
	Kr	16.29	−1.01	−1.93	−1.96	1.11	
	Xe	13.14	−0.54	−0.94	−1.37	0.32	
^3Q	Ar	20.67	−7.46	−0.24	−1.96	0.48	0.25
	Kr	18.33	−5.04	1.06	−2.47	−0.04	0.68
	Xe	16.88	−7.35	4.25	−3.48	1.34	−0.49

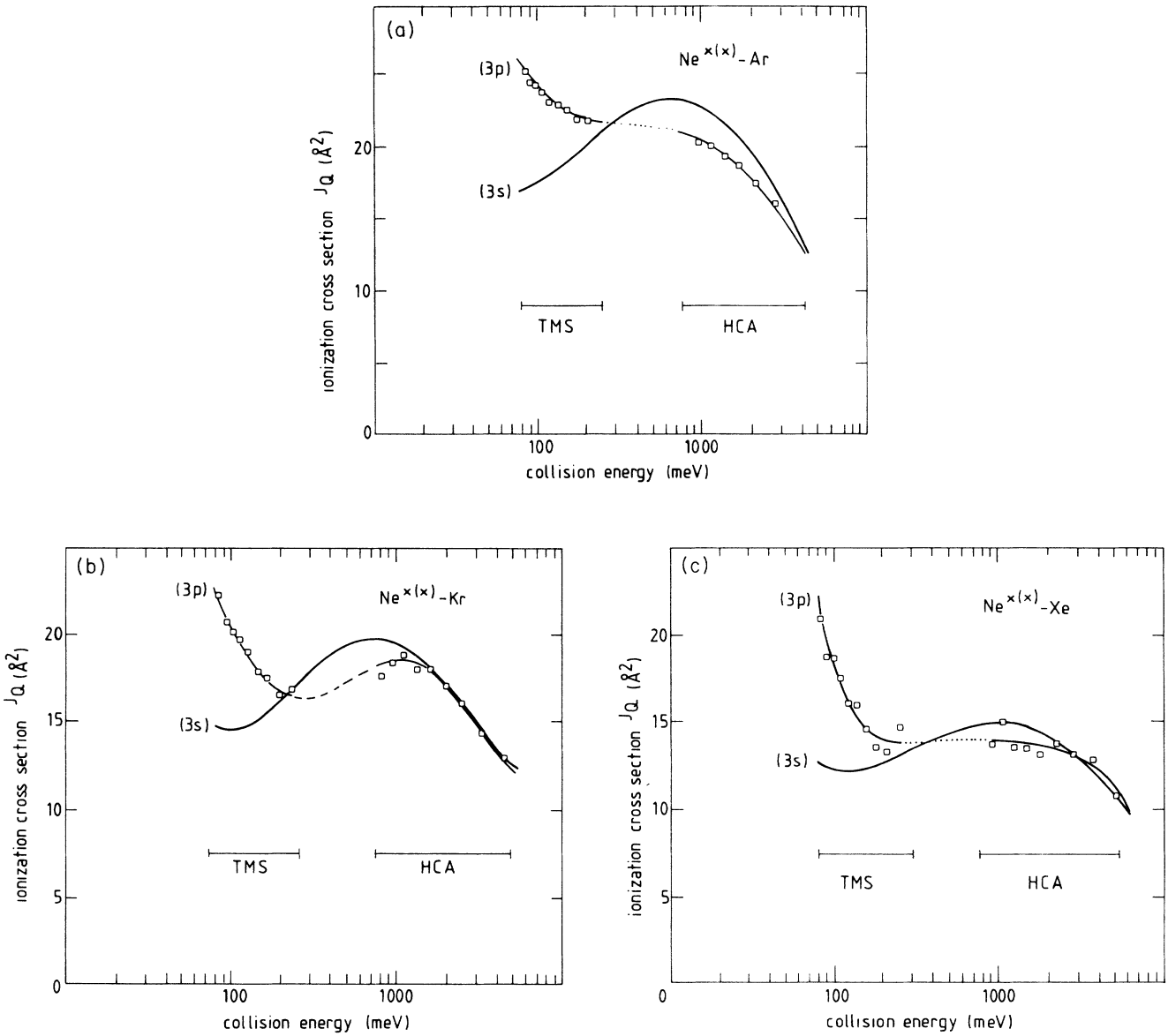

FIG. 8. The energy-resolved ionization cross section $^3Q(E)$ for the Ne**[(3p);J=3]- (a) Ar, (b) Kr, (c) Xe systems, as obtained by the least-squares analysis. For comparison we have depicted the ionization cross section $^2Q(E)$ of the metastable lower level as well.

gases. In the thermal energy range the $^3Q(E)$ cross section is larger than the $^2Q(E)$ cross section, which correlates with the smaller distance of closest approach for the Ne**[(3p)] state in comparison to the Ne*[(3s)] state. At energies in the eV range the role of the valence electron is less important and the cross sections are nearly equal, implying the same shape of the repulsive branch of the potential in this range.

The energy dependence of the polarization effect $^3Q^{|M|}(E)/^3Q(E)$ for the Ne**-Ar system is shown in Fig. 9, assuming a negligible polarization effect of the lower level in the analysis [data points; Eq. (22)]. We see a large polarization effect in the thermal energy range. In the superthermal energy range this polarization effect has almost completely vanished. For the Ne**-(Kr,Xe) systems we obtain an identical polarization effect. For the Ne**-Ar system we have performed a second analysis, using the polarization effect of the lower-level cross section, as discussed in Sec. VII A. The results of this second analysis are given in Fig. 9 as well [full lines; Eq. (21)]. The polarization effect of the $^3Q^{|M|}(E)/^3Q(E)$ cross section is even larger in this second analysis. This is not very surprising because the Ω dependence of the ionization probability for the Ne*[(3s);J=2] state has the same trend as for the upper state. In Sec. VIII we will present a semiclassical model that can explain the energy dependence of the polarization effect. The second analysis has not been performed for the Ne**-(Kr,Xe) systems because we have no information on the cross sections $^2Q^{|M|}(E)$ for these systems.

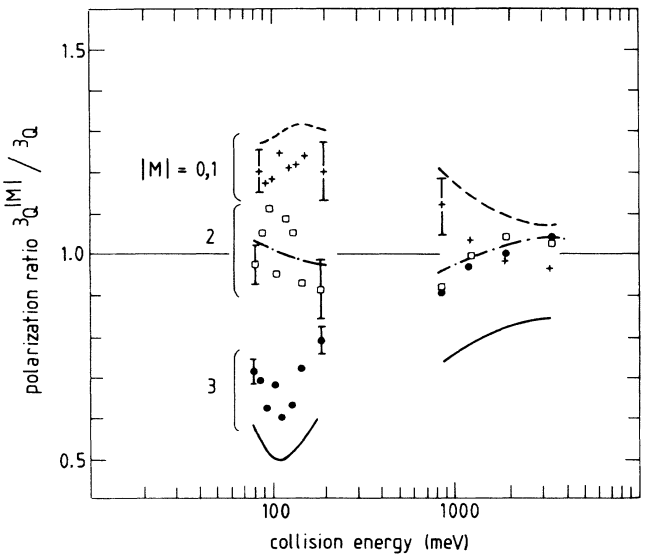

FIG. 9. The polarized-atom cross sections ${}^3Q^{|M|}(E)$ for the Ne**-Ar system scaled to the isotropic cross section ${}^3Q(E)$ as a function of the collision energy E. We observe a large polarization effect in the thermal energy range, while in the superthermal energy range the polarization effect is almost negligible.

VIII. INFLUENCE OF LOCKING

A. Semiclassical model

To calculate the polarized-atom cross sections ${}^JQ^{|M|}(E)$ from the Ω-dependent complex potentials $V_{\rm opt}(R)$ [Eq. (1)], we have extended the semiclassical model developed by Manders *et al.*[10] Basically this model is a classical trajectory calculation of the colliding particles, as already discussed in Sec. II C. The trajectory evolution for an asymptotic pure magnetic substate $\mathrm{Ne}^{**}[|J,M\rangle_g]$ colliding with an Ar atom with impact parameter b is determined from the adiabatic real potentials $V_\Omega(R)$ for the Ne**-Ar system, as calculated with the model-potential method of Sec. II A. Due to the rotation of the internuclear axis **R**, the M distribution $\sum c_M(R)|J,M\rangle$ with respect to this axis is continuously being scrambled along the trajectory, represented by the R-dependent coefficients $c_M(R)$. The average potential $V(R)$ which we use for the trajectory calculation is given by

$$V(R)=\sum_{M=-J}^{+J}[c_M(R)]^2V_\Omega(R)\Big/\sum_{M=-J}^{+J}[c_M(R)]^2\ ,$$
$$\Omega=|M|\ . \quad (24)$$

The potential is normalized by the total population $\sum_M[c_M(R)]^2$, which is less than or equal to unity, because a fraction of the $|J,M\rangle$ states is lost in the ionization process.

The $(3p)$ valence electron and the Ne $(2p)^{-1}$ core are represented by the total electronic angular momentum **J**. The evolution of the $|J,M\rangle$ quantum numbers along the trajectory is calculated with a semiclassical model, which describes both rotational coupling as well as locking. The process of intramultiplet mixing and ionization are also incorporated in the semiclassical model.

Rotational coupling describes the scrambling of the M distribution caused by the rotation of the internuclear axis. The rotational coupling is appropriate if the Ω splitting in the real potential $V_\Omega(R)$ is negligible. In this situation the Ω quantum number is not a conserved quantity and a space-fixed description of the **J** vector is applicable. For a large Ω splitting in the real potentials $V_\Omega(R)$ a torque operates on the total electronic angular momentum **J**. The Ω splitting $\Delta V_{\Omega,\Omega\pm1}(R)$ can thus be translated into a precession frequency $\omega_{\rm prec}$ of the **J** vector about the internuclear axis, as given by

$$\omega_{\rm prec}(R)=\Delta V_{\Omega,\Omega\pm1}(R)/\hbar\ . \quad (25)$$

This precession frequency $\omega_{\rm prec}(R)$ has to be compared to the angular velocity $\dot\phi(R)$ of the rotating internuclear axis. The space-fixed description of the electronic angular momentum **J** is valid in the situation that $\dot\phi(R)\gg\omega_{\rm prec}(R)$. On the other hand, if $\dot\phi(R)\ll\omega_{\rm prec}(R)$ a body-fixed description of J is necessary. There is a gradual transition between the two descriptions. In our semiclassical model, however, we have to introduce a sharp boundary between the regions where the two **J** descriptions are applicable. This locking radius R_L can be calculated with the condition

$$\omega_{\rm prec}(R_L)=f_L\dot\phi(R_L)\ , \quad (26)$$

where f_L is a locking factor. Previous calculations with a similar semiclassical model of Manders *et al.*[10] for the Ne**-He intramultiplet mixing process indicate this locking factor to be $f_L=4$.

Because the Ω splitting is not equidistant for all $[\Omega,\Omega\pm1]$ combinations, we have to determine an average Ω splitting for the neighboring Ω levels as

$$\Delta V_{\Omega,\Omega\pm1}(R)=\Delta V^{\max}(R)/J\ , \quad (27)$$

where $\Delta V^{\max}(R)$ denotes the maximum potential-energy difference between the different $|J,\Omega\rangle$ states at an internuclear distance R. The precession frequency $\omega_{\rm prec}(R)$ of the local molecular $|J,\Omega\rangle$ states about the internuclear axis is given by

$$\omega_{\rm prec}(R)=\Delta V^{\max}(R)/(J\hbar)\ . \quad (28)$$

The angular velocity $\dot\phi(R)$ is significant only for large impact parameters b, corresponding with large N quantum numbers of the orbital angular momentum of the two nuclei

$$\mathbf{N}=\mu\mathbf{g}\times\mathbf{b}=\mu v_\Phi(\mathbf{R})\times\mathbf{R}\ \text{ with }\ v_\Phi(R)=\dot\phi(R)R\ .$$

For large values $N\gg J$ the **N** vector is approximately conserved, because the total angular momentum $\mathbf{P}=\mathbf{N}+\mathbf{J}$ is a conserved quantity. This enables us to calculate the angular velocity through

$$\dot\phi(R)=|\mathbf{N}|/(\mu R^2)\simeq(N+\tfrac{1}{2})\hbar/(\mu R^2)\ . \quad (29)$$

Using Eqs. (26), (28), and (29), we can calculate a $N_{\rm lock}(R)$ value as a function of the internuclear distance

R, which serves as the locking condition

$$N_{\text{lock}}(R)+\tfrac{1}{2}=\mu R^2\Delta V^{\max}(R)/(f_L J\hbar^2)\ . \tag{30}$$

For a classical trajectory with impact parameter $b\simeq N\lambda\!\!\!^{-}$, with $\lambda\!\!\!^{-}=\hbar/(\mu,g)$, the de Broglie wavelength, the body-fixed description has to be used in the range of R values where $N\leq N_{\text{lock}}(R)$; outside this range the space-fixed description is adequate. In Fig. 10 we have depicted this $N_{\text{lock}}(R)$ value for the Ne**[$(3p)$;$J=3$]-Ar system, together with the corresponding scale of impact parameters for the collision energies $E=100$ meV and $E=1000$ meV. For an impact parameter $b=5a_0$, we see that the Ne**[$(3p)$;$J=3$]-Ar system is locked in the region $3.7<R$ (units of a_0) <10.3 for a collision energy $E=100$ meV. For a collision energy $E=1000$ meV this locking region is reduced to $6.8<R$ (units of a_0) <8.8.

When the body-fixed description is appropriate, the Ω splitting in the real potential $V_\Omega(R)$ is not negligible. In our semiclassical model each local molecular state $|J,M\rangle$ follows a unique trajectory determined by $V_\Omega(R)$ and no Ω mixing due to rotational coupling occurs. Therefore, the particle trajectory splits in $(J+1)$ trajectories when going from a space-fixed description to a body-fixed description. In the space-fixed description of the electronic angular momentum **J**, we assume that the M distribution of the local molecular states $\sum_M c_M(R)|J,M\rangle$ moves along one trajectory, which is calculated with the average real potential $V(R)$ of Eq. (23). The evolution of the local molecular M distribution $c_M(\mathbf{R})$ to a new distribution $c_M(\mathbf{R}+\Delta\mathbf{R})$ is calculated with the Wigner d function $d^J_{MM'}(\Delta\phi)$, with $\Delta\phi$ the angle in the collision plane between the two orientations $\phi(\mathbf{R})$ and $\phi(\mathbf{R}+\Delta\mathbf{R})$ of the internuclear axis, as given by

$$c_M(\mathbf{R}+\Delta\mathbf{R})=\sum_{M'=-J}^{+J} d^J_{MM'}(\Delta\phi)c_{M'}(\mathbf{R})\ . \tag{31}$$

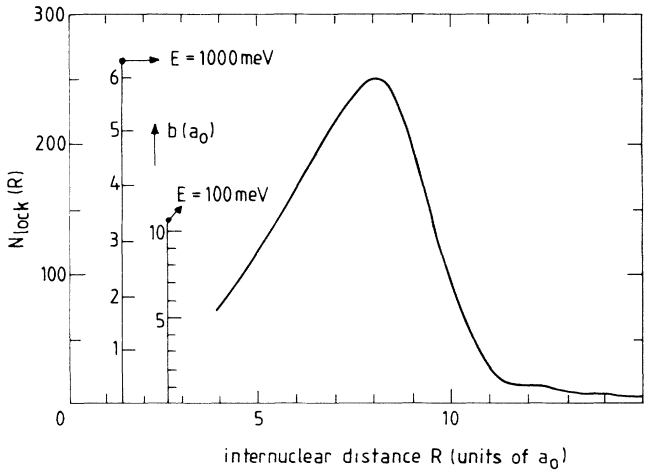

FIG. 10. The $N_{\text{lock}}(R)$ value as a function of the internuclear distance R. The impact-parameter scale is indicated for the energies $E=100$ meV and $E=1000$ meV. For low collision energies the **J** vector tends to get locked to the rotating internuclear axis, while for high energies the **J** vector keeps its space-fixed orientation.

Because the trajectory is calculated in very small steps ($\Delta R\approx 0.01a_0$), the new M distribution is calculated only when the internuclear axis has rotated over an angle larger than $\pi/20$ since the last update of the M distribution.

Because the Wigner d function takes on real values only, there is no phase information. These coherence effects lead to interference effects, which are not necessary negligible. Because the total cross section contains an integration over all impact parameter [Eq. (5)], it is to be expected that these interference effects will average out, as in the case of Ne**-He intramultiplet mixing.[10]

Rotational coupling according to Eq. (30) can be applied only if J is a good quantum number. Because we use adiabatic molecular states (Sec. II A), there can be some J mixing. This mixing of J quantum numbers is noticeable only at "avoided crossings," where radial coupling between the different Ne**[$(3p)$] states occurs. A correct description of rotational coupling of this J mixture is not possible in our semiclassical model. Only a full quantum-mechanical coupled-channel calculation incorporates this effect correctly.

The radial coupling, which occurs at the avoided crossings in the adiabatic potentials, is incorporated in our semiclassical model with Landau-Zener theory.[10,57] In this manner the inelastic process of intramultiplet mixing is taken into account. For each trajectory a crossing probability p_{cross} is calculated for going to another Ne** state of the $(3p)$ multiplet. At the crossing radius R_{cross} the Ne**[$(3p)$] state is divided over the two states according to this probability. The particle trajectory thus splits into two trajectories when passing an avoided crossing. In the case of Ne**-He intramultiplet mixing with a very large polarization effect, the semiclassical results agree very well with the experimental results and the quantum-mechanical coupled-channel calculations.[10] In our calculations for the Ne**[$(3p)$;$J=3$]-Ar system, the radial coupling to the neighboring Ne**[$(3p)$] states is taken into account as well.

The spin-orbit coupling of the σ' and the π' state of the $\text{Ne}(2p)^{-1}$ core to adiabatic Ω states is much stronger than the coupling to the continuum states through the autoionization widths $\Gamma_{\sigma'}(R)$ and $\Gamma_{\pi'}(R)$. Therefore we describe the process of ionization for each $M=\pm\Omega$ state of the M distribution $c_M(R)$ by the attenuation factor $\exp[-\Gamma_{J\Omega}(R)\Delta t/(2\hbar)]$ rather than attenuating each σ' and π' state independently. The total population of each $M=\pm\Omega$ state is then attenuated by a factor $\exp[-\Gamma_{J\Omega}(R)\Delta t/\hbar]$. The total ionization cross section ${}^JQ^{|M|}$ can then be calculated with Eq. (5). A similar expression can be given for the total cross section for intramultiplet mixing.[10]

B. Semiclassical results

To explain the observed energy dependence of the polarization effect for the Ne**[$(3p)$;$J=3$]-Ar system, we performed calculations for several collision energies E and for various locking conditions. Because the autoionization widths $\Gamma_{\sigma'}(R)$ and $\Gamma_{\pi'}(R)$ of Fig. 2 have been calculated in a one-electron approximation, the relative scal-

TABLE VI. Semiclassical results for the polarization effect ${}^3Q^{0,1}/{}^3Q^3$ as a function of the collision energy E for different locking factors f_L in comparison with the experimental results. The energy dependence of the polarization effect is best reproduced for a semiclassical locking factor of $f_L=4$.

			${}^3Q^{0,1}/{}^3Q^3$						
Energy	Experiment		Body				Space	${}^3Q$ (Å^2)	
(eV)	(a)	(b)	fixed	$f_L=2$	$f_L=4$	$f_L=8$	fixed	Expt.	$f_L=4$
0.075	1.69	2.12	3.40	1.84	1.77	1.60	1.27	24.5	32.3
0.125	1.96	2.65	4.30	1.98	1.87	1.51	1.17	23.2	28.3
0.2	1.44	1.96	5.10	2.11	1.93	1.45	1.04	21.5	23.4
0.5			5.35	2.12	1.67	1.07	0.91		19.7
1.0	1.24	1.59	5.30	2.11	1.31	0.92	0.88	20.2	16.1
2.5	1.00	1.38	4.94	1.58	0.98	0.88	0.87	16.3	12.5

[a]Neglecting the polarization effect in ${}^2Q^{|M|}$.
[b]Analyzed with the ${}^2Q^{|M|}$ results of Driessen *et al.* (Ref. 21).

ing of both functions is still undetermined. A preliminary analysis of the influence of the second electron[44,58] shows that the one-electron results should be scaled relative to each other with a factor 9 in favor of the σ' orientation. This relative scaling is supported by our semiclassical model calculations, which show that only with this modification can an agreement with the experimental data be obtained.

The autoionization widths used in our calculation are finally represented by the functions

$$\Gamma_{\sigma'}(R)\ (\mathrm{eV}) = \left[4.362 \exp(-0.658 a_0^{-1} R) \times \frac{1-\exp[(R-2.283a_0)/4.339a_0]}{1+\exp[(R-2.283a_0)/4.339a_0]} \right]^2 ,$$
$$\Gamma_{\pi'}(R)\ (\mathrm{eV}) = [0.223 a_0^{-1} R \exp(-0.869 a_0^{-1} R)]^2 . \quad (32)$$

The asymptotic behavior of the autoionization widths $\Gamma_{\sigma'}(R)$ and $\Gamma_{\pi'}(R)$ is determined by the exponential terms $\exp[-1.316a_0^{-1}R]$ and $\exp[-1.738a_0^{-1}R]$, respectively. To compare the semiclassical results with the experimental data, we have calculated the cross-section ratio

$$\mathcal{R}_{\mathrm{pol}}(E) = {}^3Q^{0,1}(E)/{}^3Q^3(E) , \quad (33)$$

with ${}^3Q^{0,1}(E) = \frac{1}{2}[{}^3Q^0(E) + {}^3Q^1(E)]$. The results are given in Table VI. The experimental value of $\mathcal{R}_{\mathrm{pol}}(E)$ is given for the analysis both with and without the Ne*[(3s)]-Ar polarization effect. Experimentally we observe a maximum in $\mathcal{R}_{\mathrm{pol}}$ at an energy $E=125$ meV. Semiclassically we can reproduce this maximum very well for a locking condition $f_L=4$. In Fig. 11 we have depicted the semiclassical ionization probability $P(b|J,M)$ as a function of the impact parameter b for two energies at this locking condition. For an energy $E=125$ meV the **J** vector becomes locked to the internuclear axis, while for an energy $E=2500$ meV the **J** vector remains space fixed. The local molecular $|J,M=\pm 3\rangle$ state has a pure π' contribution and therefore ionizes very poorly (Table I). The ionization probability $P(b|J,M)$ for the asymptotic

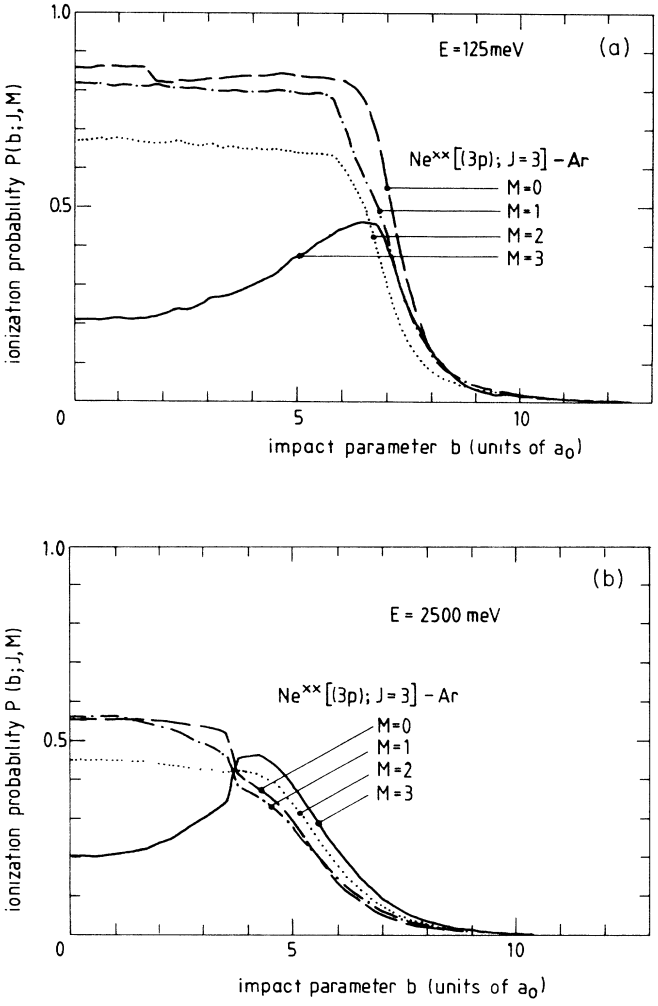

FIG. 11. The ionization probability $P(b|J,M)$ for the asymptotic magnetic substates of the Ne**[(3p);J=3] state colliding with an Ar atom. (a) For low energies the locking prevents the $|M|=3$ state from admixing a large $|M|=0,1$ contribution, leading to a small ionization probability for all impact parameters. (b) For high energies, however, rotational coupling results in a large $|M|=0,1$ contribution for large impact parameters and thus increases the ionization probability.

$|M|=3$ state remains very small for large impact parameters at an energy $E=125$ meV because of this locking, while at an energy $E=2500$ meV the ionization probability becomes significant due to rotational coupling.

The results of Table VI show that in a body-fixed situation the polarization effect is too large and has no energy dependence, whereas in a space-fixed situation the polarization effect is too small. Only for a locking condition $f_L > 1$ is a large energy dependence of the ratio $\mathcal{R}_{\text{pol}}$ observed. Therefore we conclude that the concept of locking is necessary to explain the polarization effect ${}^3Q^{0,1}/{}^3Q^3$ and its energy dependence. In our belief the energy dependence of the polarization effect gives very strong evidence for a locking condition $f_L=4$, which is also confirmed by similar results of Manders *et al.*[10] The locking factor is also confirmed by Grosser[12] in his analysis of the results of Na^+ scattering on laser-excited $Na^*(3p)$ atoms of Hertel *et al.*,[11] which also results in $f_L=4.5\pm1$ in our approach.

IX. CONCLUDING REMARKS ON LOCKING

In this paper we have strong evidence for a semiclassical picture of rotational coupling, including a reliable method for predicting an effective boundary between the limiting cases of a body-fixed or a space-fixed picture of **J**. With respect to the Ω-dependence process of ionization we have proven that a two-state basis for $\Gamma(R)$ is in fair agreement with the polarization effect. In comparison with Bussert *et al.*[5] a considerable reduction of free parameters has been achieved.

To determine the polarization effect more accurately, one has to eliminate the influence of the metastable lower level $Ne^*[(3s);J=2]$ and/or to prepare a pure M state with respect to the relative velocity **g**. In future experiments we will meet these conditions by optical excitation of single Zeeman states in a magnetic field **B** of the order of $B \simeq 300$ G.

To calculate the polarized-atom cross section ${}^JQ^{|M|}$ we perform a trajectory calculation with our semiclassical model for a $|J\rangle$ state with an asymptotic magnetic quantum number $\pm M$. In the case of $M\neq0$ the asymptotic initial state can be chosen in several ways: We can choose a pure magnetic substate $|J,M\rangle$ or a coherent sum $\frac{1}{2}\sqrt{2}[|J,M\rangle\pm|J,-M\rangle]$. The coherent sums $\frac{1}{2}\sqrt{2}[|J,M\rangle\pm|J,-M\rangle]$ correspond to electronic wave functions that are symmetric of antisymmetric with respect to reflection in the collision plane. In our experiment we measure the total cross section with contributions from the whole impact parameter range [Eq. (5)]. The azimuthal orientation of the collision plane is not restricted and a unique collision plane is not selected. Therefore the symmetric and antisymmetric wave functions will contribute equally to the polarized-atom cross section in a semiclassical approach. Only in the case of a pure magnetic substate $|J,M\rangle$ do we have azimuthal symmetry, i.e., the collision system is invariant for a rotation over an angle φ about the relative velocity **g**. An initial pure magnetic substate $|J,M\rangle$ determines the polarized-atom cross section on its own. Because the collision system is identical for all azimuthal orientations of the collision plane, the phase factor $\exp(-iM\varphi)$ does not contribute to the total cross section ${}^JQ^{|M|}$ [Sec. V B].

We have checked this assumption for the $Ne^*[(3s);J=2]$-Ar system. The trajectories are independent of the choice of the initial state, because the Ω splitting in the real potential is negligible (Sec. II C). The cross-section results in Table VII indeed show that the cross section ${}^2Q^{|M|}$ for an initial pure magnetic substate $|J,M\rangle$ is equal to the average of the cross sections ${}^2Q^{|M|}_{\pm}$ calculated with a coherent sum $\frac{1}{2}\sqrt{2}[|J,M\rangle\pm|J,-M\rangle]$ as initial state. The development of the Ω distribution is not equal for the different initial states and thus in the case of a large Ω splitting the average potential of Eq. (24) differs for the different initial states. In this situation the trajectory depends on the choice of the initial state. Thus for a large Ω splitting the average cross section $\frac{1}{2}[{}^JQ^{|M|}_{+}+{}^JQ^{|M|}_{-}]$ obtained with the coherent sums is not necessarily equal to the cross section ${}^JQ^{|M|}$ obtained with a pure magnetic substate. For the $Ne^{**}[(3p);J=3]$-Ar system the difference was found to be less than 0.2%.

For a correct interpretation of locking we have to distinguish locking of the electron orbital from locking of the total angular momentum of this orbital. To illustrate this effect we have depicted the asymptotic orientation of a p orbital $|J=1\rangle$ for three initial states in Fig. 12. The asymptotic pure magnetic substates $|1,\pm1\rangle$ are symmetric with respect to a rotation over an angle φ about the relative velocity **g** [Fig. 12 (I)]. Rotational coupling according to Eq. (31) will scramble the Ω distribution; therefore the space-fixed and body-fixed descriptions are *distinguishable*. The coherent sum $\frac{1}{2}\sqrt{2}[|1,1\rangle-|1,-1\rangle]$ state corresponds to a p_x orbital in the collision plane [Fig. 12 (II), symmetric with respect to reflection in the collision plane]. In this situation rotational coupling will admix $|\Omega=0\rangle$ states as well and the space-fixed and body-fixed descriptions are *distinguishable* also. The coherent sum $\frac{1}{2}\sqrt{2}[|1,1\rangle+|1,-1\rangle]$, however, corresponds to a p_x orbital aligned perpendicular to the collision plane [Fig. 12 (III), anti-symmetric]. Due to rotational coupling according to Eq. (31), no $|\Omega=0\rangle$ states can be obtained and therefore the space-fixed and body-fixed descriptions are *indistinguishable*. In our opinion

TABLE VII. The polarized-atom cross sections ${}^2Q^{|M|}$ for the $Ne^*[(3s);J=2]$-Ar system at a collision energy $E=100$ meV, calculated for three different initial $|J,|M|\rangle$ states.

$Ne^*[(3s);J=2]$ Initial state	${}^2Q^{\|M\|}$ (Å^2)
$\frac{1}{2}\sqrt{2}(\|2,1\rangle+\|2,-1\rangle)$; sym.(+)	15.41
$\frac{1}{2}\sqrt{2}(\|2,1\rangle-\|2,-1\rangle)$; antisym.(−)	6.29
$\|2,1\rangle$	10.85
Average value $({}^2Q^1_+ + {}^2Q^1_-)/2$	10.85
$\frac{1}{2}\sqrt{2}(\|2,2\rangle+\|2,-2\rangle)$; sym.(+)	9.94
$\frac{1}{2}\sqrt{2}(\|2,2\rangle-\|2,-2\rangle)$; antisym.(−)	9.66
$\|2,2\rangle$	9.80
Average value $({}^2Q^2_+ + {}^2Q^2_-)/2$	9.80

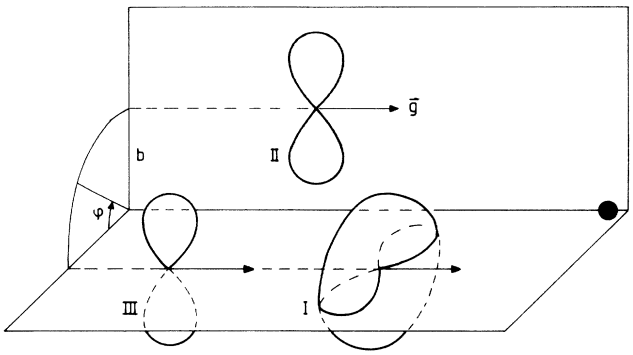

FIG. 12. The asymptotic orientation of a p orbital $|J=1\rangle$ for three initial states. The $|1,\pm1\rangle$ states have azimuthal symmetry except for a phase factor $\exp(-iM\varphi)$ (I). The symmetric state $\frac{1}{2}\sqrt{2}[|1,1\rangle-|1,-1\rangle]$ corresponds to a p_x orbital lying in the collision plane (II), while the antisymmetric state $\frac{1}{2}\sqrt{2}[|1,1\rangle+|1,-1\rangle]$ corresponds to a p_x orbital perpendicular to the collision plane (III). The coherent sums $\frac{1}{2}\sqrt{2}[|1,1\rangle\pm|1,-1\rangle]$ are not symmetric if the collision plane rotates over an angle φ.

the interpretation of Alexander and Pouilly[16] of the p_x orbital aligned perpendicular to the collision plane as a pure space-fixed situation is incorrect. In our locking picture the **J** vector will lock to the internuclear axis, which leads to a straightforward interpretation. In an orbital locking model, however, the locking interpretation is not straightforward, as we have shown above.

A limitation in our semiclassical model is the fact that the particle trajectory is restricted to the initial collision plane. In the case of an initially prepared wave function, which is antisymmetric with respect to reflection in the collision plane, it must remain antisymmetric and vice versa. For large quantum numbers N the orbital angular momentum of the two nuclei is practically conserved, because the total angular momentum $\mathbf{P}=\mathbf{N}+\mathbf{J}$ is a conserved quantity ($N \gg J$). Therefore the collision plane tilts over a very small angle and the corresponding scrambling of the symmetry of the initial prepared wave function is negligible. For small impact parameters ($N \simeq J$) this effect will become noticeable; however, the contribution of this impact-parameter range to the total cross section [Eq. (5)] is negligible. Only in a collision experiment which is selective for impact parameters, e.g., differential cross-section measurements or total cross-section measurements of endothermic processes at collision energies close to threshold, may the effect of the tilting collision plane be important.

To calculate differential cross sections with our semiclassical model for a collision of a polarized-atom with a ground-state atom, the initial asymptotic state has to be chosen very carefully. The collision plane is determined uniquely in this situation. Therefore, the coherence of the initial state is crucial for the resulting differential cross section. Another limitation of the semiclassical model with respect to differential cross sections is the fact that possible interference effects between the different magnetic substates are not likely to average out in the limited impact-parameter range involved. For total cross sections we have assumed that the interference effects will average out when we integrate over the whole impact-parameter range (Sec. VIII A).

Note added in proof. With regard to the investigations of Bussert *et al.*[5] and to our recent work[6] and the present work we add the following points: For the ionization width $\Gamma(R)$ we introduced a two-state basis, by taking into account only one electron, going into the $\mathrm{Ne}(2p)^{-1}$ hole. This simple model is sufficient to describe the polarization effect, but cannot describe final-state fine-structure branching ratios, as discussed previously by Bussert *et al.*[5] For this detailed information a more extensive model is required,[5] as proposed by Morgner.[42] In this latter model the number of free parameters is considerably larger, but was restricted to five significant transition amplitudes by Bussert *et al.*[5] in a least-squares analysis of their $\mathrm{Ne}^{**}(2p_x)+\mathrm{Ar}$ total ionization cross sections and Ar^+ fine-structure branching ratios, measured for eight $\mathrm{Ne}^{**}(2p_x,\ x=2,4-10)$ states, with $2p_x$ the usual Paschen notation of the $\mathrm{Ne}^{**}[(2p)^5(3p)]$ multiplet. We have performed a theoretical analysis using the Feshbach-projection formalism to calculate the ionization amplitudes. Basically this analysis contains the same parameters as the model of Bussert *et al.*[5] We find a set of seven significant matrix elements that are in slight but distinct disagreement with Bussert's empirical values. A detailed comparison of these two extended models is described by Driessen *et al.*[44]

ACKNOWLEDGMENTS

This work is supported by the Foundation for Fundamental Research on Matter (FOM).

*Present address: Joint Institute for Laboratory Astrophysics, University of Colarado, Boulder, CO 80309-0440.

[1]M. O. Hale and S. R. Leone, J. Chem. Phys. **79**, 3352 (1983).

[2]M. O. Hale, I. V. Hertel, and S. R. Leone, Phys. Rev. Lett. **53**, 2296 (1984).

[3]W. Bussert and S. R. Leone, Chem. Phys. Lett. **138**, 269 (1987).

[4]W. Bussert, D. Neuschäfer, and S. R. Leone, J. Chem. Phys. **87**, 3833 (1987).

[5](a) W. Bussert, T. Bregel, R. J. Allan, M. W. Ruf, and H. Hotop, Z. Phys. A **320**, 105 (1985); (b) W. Bussert, T. Bregel, J. Ganz, K. Harth, A. Siegel, M. W. Ruf, H. Hotop, and H. Morgner, J. Phys. (Paris) Colloq. **45**, C1-199 (1985).

[6]J. P. J. Driessen, F. J. M. van de Weijer, M. J. Zonneveld, L. M. T. Somers, M. F. M. Janssens, H. C. W. Beijerinck, and B. J. Verhaar, Phys. Rev. Lett. **62**, 2369 (1989); **64**, 2106 (1990).

[7]H. A. J. Meijer, T. J. C. Pelgrim, H. G. M. Heideman, R. Morgenstern, and N. Andersen, Phys. Rev. Lett. **59**, 2939 (1987); J. Chem. Phys. **90**, 738 (1989).

[8]M. P. I. Manders, J. P. J. Driessen, H. C. W. Beijerinck, and B. J. Verhaar, Phys. Rev. Lett. **57**, 1577 (1986); **57**, 2472 (1986); Phys. Rev. A **37**, 3237 (1988).
[9]M. P. I. Manders, W. M. Ruyten, F. van de Beucken, J. P. J. Driessen, W. J. T. Veugelers, P. H. Kramer, E. J. D. Vredenbregt, W. B. M. van Hoek, G. J. Sandker, H. C. W. Beijerinck, and B. J. Verhaar, J. Chem. Phys. **89**, 4777 (1988).
[10]M. P. I. Manders, W. B. M. van Hoek, E. J. D. Vredenbregt, G. J. Sandker, H. C. W. Beijerinck, and B. J. Verhaar, Phys. Rev. A **39**, 4467 (1989).
[11]I. V. Hertel, H. Schmidt, A. Bähring, and E. Meyer, Rep. Prog. Phys. **48**, 375 (1985).
[12]J. Grosser, Comments At. Mol. Phys. **21**, 107 (1988).
[13]J. Grosser, Z. Phys. D **3**, 39 (1986).
[14]A. Bähring, E. Meyer, I. V. Hertel, and H. Schmidt, Z. Phys. A **320**, 141 (1985).
[15]A. Bähring, I. V. Hertel, E. Meyer, W. Meyer, N. Spies, and H. Schmidt, J. Phys. B **17**, 2859 (1984).
[16]M. H. Alexander and B. Pouilly, in *Selectivity in Chemical Reactions,* edited by J. C. Whitehead (Kluwer, Dordrecht, 1988), p. 265.
[17]B. Pouilly and M. H. Alexander, J. Chem. Phys. **86**, 4790 (1987).
[18]V. Aquilanti, G. Grossi, and A. Lagana, Nuovo Cimento B **63**, 7 (1981).
[19]V. Aquilanti, G. Liuti, F. Pirani, and F. Vecchiocattivi, J. Chem. Soc. Faraday. Trans. **85**, 955 (1989).
[20]T. Bregel *et al.*, in *Electronic and Atomic Collisions,* edited by D. C. Lorents, W. E. Meyerhof, and J. R. Peterson (North-Holland, Amsterdam, 1986), p. 577.
[21]J. P. J. Driessen, H. J. L. Megens, M. J. Zonneveld, H. A. J. Senhorst, H. C. W. Beijerinck, and B. J. Verhaar, Chem. Phys. (to be published).
[22]S. Iwata, Chem. Phys. **37**, 251 (1979).
[23]J. S. Cohen and B. Schneider, J. Chem. Phys. **61**, 3230 (1974).
[24]F. Masnou-Seeuws, M. Philippe, and P. Valiron, Phys. Rev. Lett. **41**, 95 (1978).
[25]D. Hennecart and F. Masnou-Seeuws, J. Phys. B **18**, 657 (1985).
[26]R. Düren, E. Hasselbrink, and E. Moritz, Z. Phys. A **307**, 1 (1982).
[27]W. Bussert, Ph.D. thesis, Universität Kaiserslautern, West Germany, 1985.
[28]D. Hausamann and H. Morgner, Mol. Phys. **54**, 1085 (1985).
[29]R. W. Gregor and P. E. Siska, J. Chem. Phys. **74**, 1078 (1981).
[30]E. R. T. Kerstel, M. F. M. Janssens, K. A. H. van Leeuwen, and H. C. W. Beijerinck, Chem. Phys. **119**, 325 (1988).
[31]H. Morgner, Comments At. Mol. Phys. **11**, 271 (1982).
[32]R. J. Bieniek, Phys. Rev. A **18**, 392 (1978).
[33]D. M. Jones and J. S. Dahler, Phys. Rev. A **37**, 2916 (1988).
[34]A. P. Hickman, A. D. Isaacson, and W. H. Miller, J. Chem. Phys. **66**, 1483 (1977).
[35]A. P. Hickman and H. Morgner, J. Chem. Phys. **67**, 5484 (1977).
[36]E. Clementi, Tables in Atomic Functions, supplement to IBM J. Res. Dev. **9**, 2 (1965).
[37]H. Haberland (private communication).
[38]M. J. Verheijen and H. C. W. Beijerinck, Chem. Phys. **102**, 255 (1986).
[39]J. P. C. Kroon, A. Cottaar Haverkorn, and H. C. W. Beijerinck, Chem. Phys. **103**, 119 (1986).
[40]K. Gillen, P. R. Jones, and T. Tsuboi, Phys. Rev. Lett. **56**, 2610 (1986).
[41]H. Hotop, J. Lorenzen, and A. Zastrow, J. Electron Spectrosc. Relat. Phenom. **23**, 347 (1981).
[42]H. Morgner, J. Phys. B **18**, 251 (1985).
[43]G. Weiser and P. E. Siska, J. Chem. Phys. **85**, 4746 (1986).
[44]J. P. J. Driessen, S. S. Op de Beek, L. M. T. Somers, H. C. W. Beijerinck, and B. J. Verhaar (unpublished).
[45]D. Hausamann, Ph.D. thesis, Albert-Ludwigs-Universität Freiburg, West Germany, 1986.
[46]F. T. M. van den Berg, J. H. M. Schonenberg, and H. C. W. Beijerinck, Chem. Phys. **115**, 359 (1987).
[47]M. J. Verheijen, H. C. W. Beijerinck, and N. F. Verster, Rev. Sci. Instrum. **56**, 62 (1985).
[48]M. J. Verheijen, H. C. W. Beijerinck, W. A. Renes, and N. F. Verster, J. Phys. E **17**, 1207 (1984).
[49]P. L. Knight and P. W. Milloni, Phys. Rep. **66**, 21 (1980).
[50]W. Bussert *et al.*, Chem. Phys. Lett. **95**, 277 (1983).
[51]J. P. J. Driessen, M. P. I. Manders, F. J. M. van de Weijer, G. J. Sandker, W. Boom, H. C. W. Beijerinck, and B. J. Verhaar (unpublished).
[52]U. Fano and J. H. Macek, Rev. Mod. Phys. **45**, 553 (1973).
[53]A. Fischer and I. V. Hertel, Z. Phys. A **304**, 103 (1982).
[54]E. J. W. van Vliembergen, E. J. D. Vredenbregt, G. H. Kaashoek, J. P. J. Jaspar, M. M. M. van Lanen, M. F. M. Janssens, M. J. Verheijen, and H. C. W. Beijerinck, Chem. Phys. **114**, 117 (1987).
[55]C. P. J. W. van Kruijsdijk, Internal Report No. EUT-VDF/NO 85-04, Eindhoven University of Technology, Eindhoven, The Netherlands, 1985 (unpublished) (in Dutch).
[56]*Handbook of Mathematical Functions,* Natl. Bur. Stand. Appl. Math. Ser. No. 55, edited by M. Abramowitz and I. Stegun (U.S. GPO, Washington, D.C., 1965).
[57]E. E. Nikitin, in *Chemische Elementar Prozesse,* edited by H. Hartmann and J. Heidelberg (Springer-Verlag, Berlin, 1968).
[58]H. C. W. Beijerinck, J. P. J. Driessen, L. M. T. Somers, and B. J. Verhaar, Twelfth International Symposium on Molecular Beams, Book of Abstracts, Perugia, 1989, edited by V. Aquilanti (unpublished), p. 390.